

The Pennsylvania State University

The Graduate School

College of Engineering

**ANALYSIS OF THE THERMAL PROPERTIES OF
ZINC OXIDE USING THE ReaxFF REACTIVE FORCE FIELD**

A Thesis in

Mechanical Engineering

by

Arvind Krishnasamy Bharathi

© 2010 Arvind Krishnasamy Bharathi

Submitted in Partial Fulfillment
of the Requirements
for the Degree of

Master of Science

December 2010

The thesis of Arvind Krishnasamy Bharathi was reviewed and approved* by the following:

Adri van Duin
Assistant Professor, Mechanical Engineering
Thesis Advisor

Amanul Haque
Professor, Mechanical Engineering

Karen Thole
Professor
Head of the Department, Mechanical Engineering

*Signatures are on file in the Graduate School

ABSTRACT

The objective of this paper is to determine the thermal conductivity of Zinc Oxide nanowire by equilibrium and non-equilibrium molecular dynamics (EMD and NEMD) simulations using the ReaxFF reactive force field [19]. While EMD uses an equilibrated system and statistical averaging; NEMD uses cooling/heating rates in order to calculate the conductivity. The validity of the methods is first verified using Argon as a test case. The thermal conductivity of Argon thus calculated is compared with the results obtained by Bhowmick and Shenoy [69]. We then study the effects of system size using EMD method and effects of periodic boundary conditions - 1D, 2D and bulk variation of conductivity with temperature are analyzed using NEMD simulations. The results obtained compare favorably with those measured experimentally [46][47]. This indicates that the EMD and NEMD methods are reliable alternatives to the traditional Green-Kubo approach [51]; which is traditionally employed in MD-based thermal conductivity determination. In conjunction with ReaxFF, these methods are computationally cheaper than the Green-Kubo method and can be used to determine the thermal conductivity of materials involved in surface chemistry reactions such as catalysis and sintering.

The effect of chemistry on the thermal conductivity of Zinc Oxide is studied. Sintering is taken as the chemical process of interest and is simulated using ReaxFF force field for Zinc Oxide [58] in the presence of water. Effect of sintering temperature is also observed. A clear drop in the conductivity of Zinc Oxide due to the formation of

hydroxyl grain-boundaries between the different Zinc Oxide clusters is noted. However, this deterioration is smaller when we use higher sintering temperatures.

Due to a relatively small number of atoms (960) and the non-homogeneous nature of the cluster; (mix of Zinc Oxide and water) the error bars on thermal conductivity are large. This indicates the need for performing larger-scale simulations in order to determine the effect of sintering on thermal-conductivity more accurately.

TABLE OF CONTENTS

ABSTRACT.....	iii
LIST OF FIGURES	vii
LIST OF TABLES	ix
ACKNOWLEDGEMENTS.....	x
Chapter 1 Introduction	1
1.1 Introduction to Nanoscience	1
1.2 Historical perspective	1
1.3 Applications and limitations of nanotechnology	4
1.4 General simulation methods	5
1.5 History of computer simulation.....	5
1.6 Molecular Dynamics.....	8
1.6.1 Fundamentals of Molecular Dynamics.....	9
1.7 The Molecular Dynamics algorithm.....	11
1.7.1 Initialization.....	12
1.7.2 Energy and force calculations	12
1.7.3 Integration of Newtons equation of motion.....	15
1.7.4 Equilibration	16
1.8 Simulating bulk systems: Periodic Boundary Conditions	16
1.9 Types of ensembles.....	18
1.9.1 Micro-canonical ensemble.....	18
1.9.2 Canonical ensemble.....	19
1.9.2.1 Berendsen's thermostat	19
1.9.3 Isothermal/Isobaric ensemble	21
1.9.4 Grand canonical ensemble	21
1.10 Types of Force fields	22
1.10.1 Non-reactive force fields	24
1.10.2 Reactive force field.....	25
1.11 ReaxFF reactive force field	26
1.11.1 Features of ReaxFF.....	26
1.11.2 Force field training and optimization	30
1.12 Zinc Oxide	30
1.12.1 Crystal structure.....	33
1.12.2 Applications.....	34
Chapter 2 Theory of thermal conductivity and ReaxFF	37
2.1 Kinetic theory of gases	37
2.1.1 Assumptions	38

2.1.2 Mean free path.....	39
2.1.3 Thermal conductivity.....	43
2.2 Phonon theory.....	44
2.2.1 Specific heat of solids.....	44
2.2.2 Phonon scattering.....	45
2.3 Literature review of thermal transport in Zinc Oxide.....	49
2.3.1 Synthesis of Zinc Oxide.....	49
2.3.2 Thermal conductivity of Zinc Oxide.....	50
2.3.3 Zinc Oxide force fields.....	54
Chapter 3 Thermal conductivity simulations and results of Zinc Oxide.....	56
3.1 Steady State Non-Equilibrium method (SS-NEMD).....	56
3.2 Transient Non-Equilibrium method (T-NEMD).....	60
3.3 Thermal conductivity simulations.....	67
3.3.1 Solid Argon simulations.....	67
3.3.2 Zinc Oxide simulations.....	68
3.4 Results and discussions.....	72
3.4.1 Thermal conductivity of Argon.....	72
3.4.2 Thermal conductivity of Zinc Oxide.....	74
3.5 Sintering.....	79
3.5.1 Simulation.....	79
3.5.2 Results and discussion.....	82
Chapter 4 Conclusions.....	87
4.1 Nanowire simulations.....	87
4.2 Sintering simulations.....	90
4.3 Future work.....	91
BIBLIOGRAPHY.....	93
APPENDIX A.....	99
APPENDIX B.....	102
APPENDIX C.....	105

LIST OF FIGURES

Figure 1.1: Lycurgus cup: Dated 800 B.C., the di-chromism of this cup is due to nano-composite materials	2
Figure 1.2: Advantage of simulation: Ability to model difficult experiments - Phase diagram of different metals inside the earth's crust	7
Figure 1.3: Advantage of simulation: Predicting experimental results - <i>ITER Tokamak Plasma containment</i>	7
Figure 1.4: Principle of Ergodicity: Ensemble averaging and time-averaging are equivalent.....	11
Figure 1.5: Flow chart showing steps involved in Molecular Dynamics	13
Figure 1.6: Lennard-Jones potential: Potential energy Vs Distance.....	14
Figure 1.7: Simulation of bulk systems: Periodic Boundary Conditions.....	17
Figure 1.8: Hierarchy of different scales of simulation	23
Figure 1.9: Bonded interactions (Top – bond energy, Right - Valence angle energy, Bottom – Torsion energy).....	23
Figure 1.10: Reactive (describes brown and green states), Non-reactive force fields (describes brown states only).....	25
Figure 1.11: Variation of bond order with interatomic distance.....	28
Figure 1.12: Computational expense of ReaxFF in comparison with Quantum Mechanical methods	29
Figure 1.13: Elements currently described by ReaxFF reactive force field	29
Figure 1.14: Diverse growth forms of Zinc Oxide: Nanorods/nanowires, Nanobelt, Nanocomb, Nanohelix, Nanoring, Nanocage (from left to right).....	32
Figure 1.15: Surface area enhancement of materials at the nanoscale.....	33
Figure 1.16: Zinc Oxide crystal structure: (Top left) Hexagonal Wurtzite, (Top right) Cubic Zinc Blende, (Bottom) Cubic Rock salt.....	35
Figure 2.1: Sphere of exclusion: Minimum collision distance between atoms determines mean free path.....	40

Figure 2.2: Survival equation: Number of smaller bullet molecules that do not collide with larger target molecules.....	41
Figure 2.3: 1D chain of atoms exhibiting vibrational characteristics	46
Figure 3.1: Schematic representation of the SS-NEMD method (Red represents the hotter regions, blue shows the colder regions).....	57
Figure 3.2: Temperature profile obtained from SS-NEMD analysis, the marked region represents the temperature profile that is used for analysis.....	60
Figure 3.3: Linear curve fit for temperature zone 1(top), zone 2(center), zone 3 (bottom) obtained from SS-NEMD analysis	61
Figure 3.4: Systems used in T-NEMD method.....	63
Figure 3.5: Temperature profile obtained on curve fitting MD data, each profile represents the temperature distributions at different times.....	64
Figure 3.6: Goodness of model for MD data.....	65
Figure 3.7: Radial distribution function for amorphous and crystalline Zinc Oxide, Zn-O pair.....	71
Figure 3.8: Variation of conductivity of Zinc Oxide (Crystalline, Amorphous) with Surface area to Volume ratio	75
Figure 3.9: Comparison of thermal conductivity of Zinc Oxide method for 1D, 2D and 3D periodic boundary conditions using T-NEMD.....	77
Figure 3.10: Sample preparation for sintering simulation.....	81
Figure 3.11: Sintered structures at the end of simulation at different anneal temperatures.....	82
Figure 3.12: Cluster showing the number of grain boundaries, in terms of relative weight, between the heat source and itself	83
Figure 3.13: Variation of Temperature Vs Time with sintering temperature.....	84
Figure 3.14: Variation of Temperature Vs Time with number of grain boundaries....	85
Figure 3.15: Variation of Thermal conductivity Vs Temperature (Sintered and unsintered cases).....	85

LIST OF TABLES

Table 3.1: System specifications of models used in Zinc Oxide SS-NEMD method	68
Table 3.2: System specifications of Zinc Oxide models used for T-NEMD method.....	70
Table 3.3: Thermal conductivity of Argon using T-NEMD method	73
Table 3.4: Thermal conductivity of Argon cube using T-NEMD method.....	73
Table 3.5: Thermal conductivity of Zinc Oxide using SS-NEMD method.....	73
Table 3.6: Thermal conductivity of Zinc Oxide for different periodic boundary conditions using T-NEMD	77
Table 3.7: Thermal conductivity of the sintered cluster	86
Table 3.8: Thermal conductivity of the unsintered cluster.....	86

ACKNOWLEDGEMENTS

First and foremost, I would like to thank my parents for everything they have done to see me reach this stage. Their constant support gave me the strength to come to the United States and survive with financial and mental integrity.

I am grateful to Dr. Adri van Duin, who has been a great advisor and guide; during the past two years at Penn State. I would also like to thank him for entrusting me with this project as it has helped me in learning more about the field of engineering and espousing an interest in research. He has helped me evolve as a student and as a passionate learner.

I also thank Dr. Aman ul Haque for agreeing to be on my thesis committee. His guidance during the early stages of my project helped me in set project goals and defined new avenues for me to work on. His valuable suggestions on my thesis have helped improve the clarity and completeness of this document.

A special thanks to Amar Kamat for helping me out in performing simulations related to my thesis. He has also been of great help in reviewing my papers and performing calculations. I thank Dr. Mike Russo and Kaushik Joshi for his guidance with molecular dynamics related software, Satyam and Shashank for all their inputs and their presence which has made the past two years a most enjoyable learning experience.

Chapter 1

Introduction

1.1 Introduction to Nanoscience

Nanoscience is defined as the ability to observe study, manipulate and manufacture materials at the nanoscale [1]. Though still in its infancy, this field has grown in leaps and bounds over the past fifty years. Thousands of nano-designs have already been identified for engineering and medical applications. The doubling rate of the number of these designs is just two years [1]. This has been possible due to the fact that we can vary the properties of nanomaterials considerably which is generally not possible with bulk materials. This is because; the surface area and quantum effects, which are negligible at the macroscale, play an important role at the nanoscale. Thus the birth of a new science with infinite permutations and combinations is what makes the realm of 'Nano' both intriguing and exciting.

1.2 Historical perspective

Nanoscience has been an anonymous part of human history. Relics from the past have shown our ability to work with nanomaterials even though it did not exist as a concept until the mid-twentieth century. Perhaps the oldest and most famous relic is the Lycurgus cup which shows the King Lycurgus being dragged in to the underworld by the



Figure 1.1: Lycurgus cup: Dated 800 B.C., the di-chromism of this cup is due to nano-composite materials

maenad Ambrosia [2]. This cup, which is dated to 800 B.C., is actually a nano-composite material comprising of gold, silver and copper. The splendid dichromism of the composite renders the cup green when illuminated from the outside and crimson red when illuminated from the inside. Romans are known to have created beautiful stained windows by adding metals and metal oxides. Ancient Chinese cultures are also known to have used similar methods in making porcelain inlaid with gold.

In more recent history, the introduction of newer materials, that have revolutionized the way humans live, can also be attributed to such nano-composite materials. The discovery of steel in the industrial age (1600 A.D.) changed the way buildings were constructed and added muscle to militaries. Invention of vulcanized rubber in the 1800s added a new flexibility to automobiles. The first mention of the distinguishing concept of nanoscience and nanotechnology was made by James Maxwell in 1867 [5] [6]. As a thought experiment, he introduced the concept of ‘Maxwell’s demon’ which would be capable of handling individual molecules’ [3]. More information on nano materials was revealed through the study of gold sols made by Zsigmondy where he characterized particles in the size of 10nm and lesser using the ultra microscope [7] in

1914. Many important discoveries characterizing nanomaterials happened in the field related to interface and colloidal chemistry during the 20th century. In 1920, Irvin Langmuir and Katharine B Blodgett introduced the concept of the molecular monolayer for which Langmuir was awarded the Nobel Prize. This later paved way to experimental measurement of surface forces in the 1950s.

The famous speech given by the physicist Richard Feynman ‘There’s plenty of room at the bottom’ [8] touched up on the topic of nanotechnology in 1959 in which he described how specific tools could be used to develop high performance mini particles [10]. The term ‘nanotechnology’ was first coined by Norio Taniguchi of the Tokyo Science University in his review titled- ‘*On the Basic Concept of ‘Nano-Technology’*’ [9] in 1974. During the 1980s, nanoscience got a boost from the birth of cluster science and the invention of the scanning tunneling microscope (STM) [11]. This led to the discovery of fullerenes and the revolutionary carbon nanotubes which enabled scientist to characterize nanomaterials better. This resulted in new methods of synthesizing semiconductor crystals and a rapid increase in the number of semiconductor nanoparticles or quantum dots on microchips in accordance with the Moore’s law.

Dr.Drexler’s initiative in 1980s decade led to the wider acceptance of nanotechnology through the setting up of Drexel Nanotechnology Institute. In the latter half of this decade, the need to fund research in this field was recognized by the US government and so the U.S National Nanotechnology Initiative was formed. Since then a research and development in this area has been more focused.

1.3 Applications and limitations of nanotechnology

Currently, as we stand, nanotechnology holds great promises in many diverse fields. Perhaps the greatest promise is in the field of medicine where nanobots can be used to cure diseases and may be even attack and repair cancerous cells. Another closely related use is in drug delivery systems that will make sure the drugs are released at the right place and time. Nanotechnology can play an important role part in surgery in the form of guided lasers and artificial transplants and in enhancing bone repair [10]. Catalysts can be used to purify the air thereby enhancing air quality. Cost effective electronic equipment can be made more powerful and versatile. Newer fuels and longer lasting batteries; all lie within the realm of nanotechnology. The more daring speculations that scientist have made are use of nanotechnology in anti-aging thereby increasing life expectancy and may be even space travel for everyone

In spite of the vast possibilities, this new concept has some downsides. The foremost is nanopollution which is a general term that refers to the wastes left by nano machines. This arises from the fact that nanoparticles, once released, are hard to control. They may be ingested along with air, food or water and cause unknown diseases. Another major concern is that they would interrupt the lifecycles of micro organisms which are very important for the maintaining an ecological balance.

1.4 General simulation methods

Scientists have devised a number of methods to study nanomaterials including experimental and simulation approaches. While experimental methods have been around for centuries; simulation methods gained wide popularity only recently with the advent of high speed computing. This section gives a brief history of computing followed by an introduction to common techniques such as Monte Carlo and Molecular dynamics. The section concludes with a prelude to ReaxFF reactive force field.

1.5 History of computer simulation

During World War II, computers were used to perform heavy computational tasks and code breaking. During this era, machines were mostly restricted to government and not available to the general public. However, after the war, they became available for non-military use as well. When the MANIAC (*Mathematical Analyzer, Numerical Integrator, and Computer* or *Mathematical Analyzer, Numerator, Integrator, and Computer*) was built, many scientists were invited to perform computations on it in order to test its algorithms and logic structures. Soon many more such supercomputers were built and which helped simulation methods gain popularity.

The next major initiative in the United States was the Advanced Simulation and Computing Initiative Program (ASCI). This program was originally intended to simulate a nuclear blast in view of the nuclear test ban treaty in 1992. Later on this project expanded its scope to cover a wider range of computer simulation initiatives. The

Japanese built the NEC earth simulator, a super computer in order to predict weather in May 2002.

Industries were not far behind. Even today they are responsible for a third of research that goes on in this field. Companies such as Motorola, Intel, Siemens, GM and other automobile companies are among the forerunners in modeling based on the fundamental principles of quantum mechanics.

Nowadays, simulations are being used by scientists in many diverse fields. Chemists use it to simulate reactions, biologists use it to simulate enzyme binding, mechanical engineers use it to study combustion and so the list goes on. There are many reasons why simulations have become so popular. Some of them are mentioned below:

1. Ability to model difficult experiments – Consider an experiment where one is interested to find the phase composition on metals like iron and nickel inside the earth's crust (Fig. 1.2). Making an experimental setup for such a case will be extremely difficult and hazardous. However, generating the high temperature and pressure using computer is safe and inexpensive.

2. Predicting experimental results – The International Thermo-Nuclear Experimental Reactor (ITER) is an international endeavor to generate power from fusion (Fig. 1.3). In such cases, where the theory is new and requires testing, it would be risky to directly test theory with full size models. Hence engineers prefer to simulate the design and make sure it delivers desired results before actually building a full-scale model.

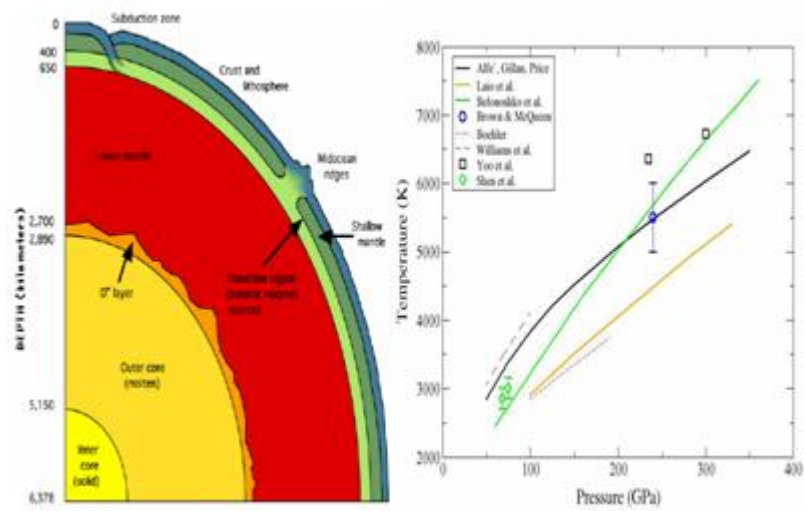


Figure 1.2: Advantage of simulation: Ability to model difficult experiments - Phase diagram of different metals inside the earth's crust

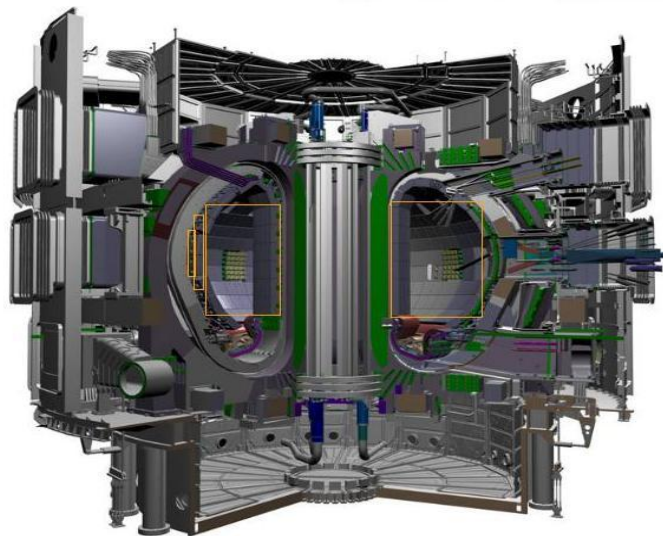


Figure 1.3: Advantage of simulation: Predicting experimental results - *ITER Tokamak Plasma containment*

3. Aids in visualization – This is one of the major advantages of using simulation. One can actually see reactions taking place. Reactions like catalysis and mechanical phenomena like buckling and thermal bending can be seen which helps in gaining physical insight.

4. Measurement of properties – One of the most difficult aspects to setup in an experiment is to devise a method to obtain the property one needs. For example, if one is interested in determining the presence of a particular radical during combustion, it would be extremely difficult to do this. However, in a simulation, one can program in order to obtain the desired output.

The benefits above mentioned are just a few. There are many more reasons why this method is becoming hugely popular. Of course, we must realize even though simulations have many significant advantages, they will not likely replace experimental methods in the near future. They are to complement them in places where experiments cannot be performed. Simulations are developed to test theory and once a good comparison is made, then it can be extended to study other related systems.

1.6 Molecular Dynamics

Molecular Dynamics (MD) simulation is one of methods used for atomistic-scale simulations. Development of molecular dynamics started only half a century ago once use of computers started to spread among academia and developed contemporarily along with other atomistic simulation methods. The molecular dynamics method was first introduced by Alder and Wainwright in the late 1950's [32][33] to study the interactions of hard spheres. The next major advance was in 1964, when A. Rahman carried out the first simulation using a realistic potential for liquid argon [34]. The first molecular dynamics simulation of a more complex system was done by Rahman and Stillinger in

their simulation of liquid water in 1974[35]. The first protein simulations appeared in 1977 with the simulation of the bovine pancreatic trypsin inhibitor (BPTI) [36]. Today in the literature, one routinely finds molecular dynamics simulations in a wide variety of fields from chemistry to mechanics and even physics and mathematics. Over the years, many algorithms have been developed and simulation techniques now exist to model a large number of experimental as well as hypothetical situations.

1.6.1 Fundamentals of Molecular dynamics

Molecular dynamics is based on the premise that nuclei behave as classical particles. Though this is not exactly accurate; but it has been found to work well for many elements. The three fundamental ideas behind the MD technique are as follows:

1. Newton' second law of motion –

$$\frac{\partial^2 \vec{r}}{\partial t^2} = F(\vec{r}) \quad (1.1)$$

2. Conservation of energy –

$$\frac{d}{dx} \left(\frac{1}{2} m v^2 + U(r) \right) = 0 \quad (1.2)$$

We relate the velocity, which is a mechanical property to a thermodynamic property using the Eqn 1.3. This equation provides an important link between the property of the molecule (through N_f - the degrees of freedom) and controllable parameters like the temperature.

$$\sum_{i=1}^N \frac{1}{2} m_i v_i^2 = \frac{3}{2} N_f k_b T \quad (1.3)$$

3. Principle of Ergodicity –

Consider Fig. 1.4. Suppose we are interested in calculating the probability of getting the number ten on spinning a roulette wheel. We can do this in one of two ways. We could either spin a single roulette wheel 100 times or spin a 100 roulette wheels once. Since each spin is mutually exclusive, the results are independent and hence the probability calculated both ways are equivalent. The former method is called time averaging while the latter is called space or ensemble averaging. The principle of ergodicity states that time averaging and space averaging are equivalent.

In molecular dynamics, just like in an experiment, the system is subject to statistical noise and hence in order to get good results, we can time average or ensemble average the desired properties to get meaningful results. For time averaging, a single simulation has to run for a long time period while in ensemble averaging; a large of number of equivalent systems are run for a relatively shorter period. Since, the systems are equivalent, their behavior also will be similar. Thus data from all these different simulations can be treated as though they are from the single system. Both methods have their advantages. It is up to the user to decide what type of averaging will give better results. The work presented uses time averaging techniques only.



Figure 1.4: Principle of Ergodicity: Ensemble averaging and time-averaging are equivalent

1.7 Molecular Dynamics algorithm

Fig. 1.5 shows the schematic representation of the Molecular Dynamics algorithm. The major steps involved are:

I Initialization

II Energy and force calculations

III Integration of Newton's equations of motion

IV Equilibration

Each of these steps has been described below in detail.

1.7.1 Initialization

The first step is initialization where molecules are randomly placed in a periodic box at a minimum distance away from each other. Next, random velocities are assigned

to them. These velocities can either be truly random or have a Maxwellian distribution. In any case, the velocities should be such that the net momentum of the system is zero. Next, the velocities are scaled in order to obtain the desired temperature. Scaling is done using Eq. 1.3. Now that the current positions and velocities of all the molecules are known, we determine the position of the particle at the previous time step using

$$x_{i-1} = x_i - vdt \quad (1.4)$$

1.7.2 Energy and force calculations

Next, the force on the particles needs to be calculated. For this, the concept of potential is introduced. A potential describes the energy of a particle due to its interaction with all other particles. These interactions can be classified, based on the range of their significance, into bonded/ short-range and non-bonded/long-range interactions. The non-bonded interactions are van der Waals forces and electrostatic forces. Bonded interactions include force terms that espouse from bond formation such as bending and torsion due to bond strain.

$$\phi(R_{ab}) = 4\varepsilon \left[\left(\frac{\sigma}{R_{ab}} \right)^{12} - \left(\frac{\sigma}{R_{ab}} \right)^6 \right] \quad (1.5)$$

From Eq. 1.5, we see that the potential depends only on the distance between the molecules. Another point to be noted is that they take into account the interactions of only two atoms a time (two body potentials).

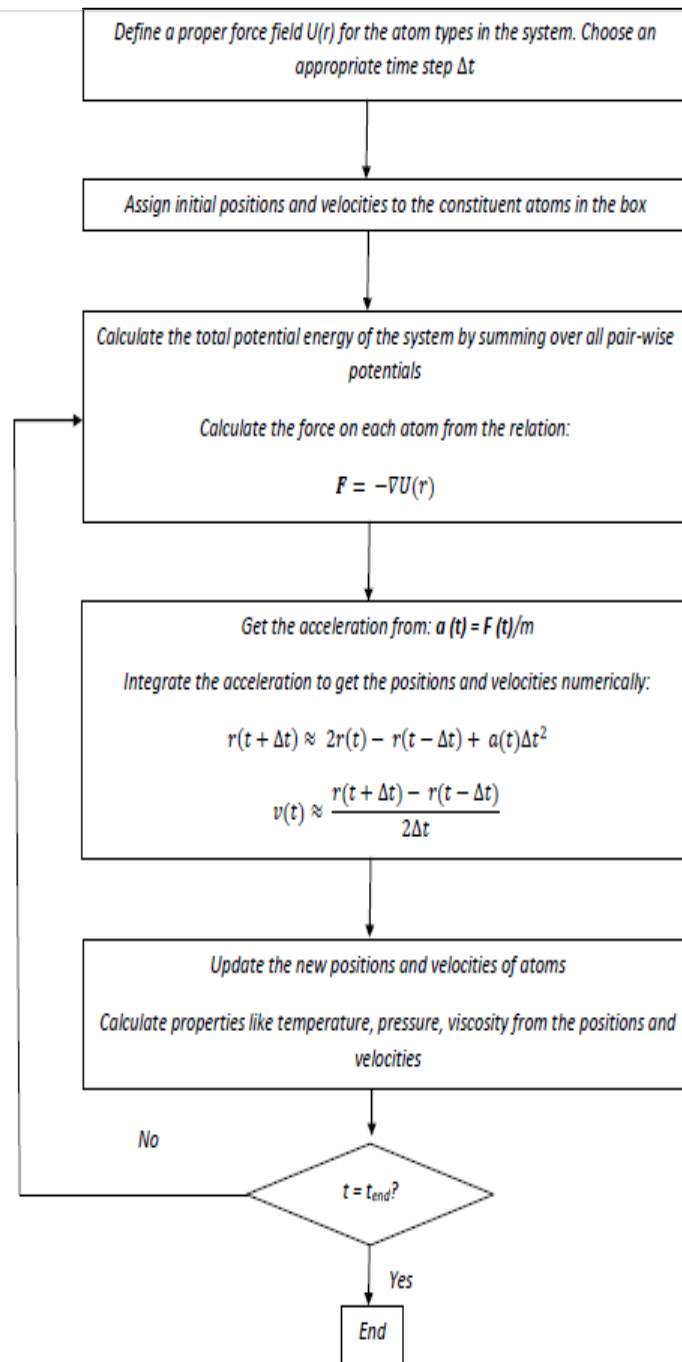


Figure 1.5: Flow chart showing the algorithm of Molecular Dynamics

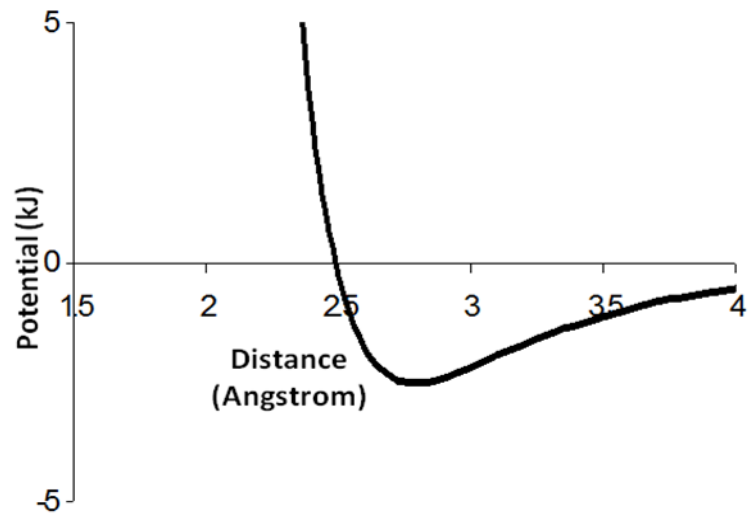


Figure 1.6: Lennard-Jones potential: Potential energy Vs Distance

There are many other potential functions such as three-body potentials and cluster potentials which take more than two atoms, in to account, at a time. Currently, there is no single universal potential that suits all cases; rather there are potential functions that describe some cases better than the others depending on the case study.

Thus the potential energy of one particle due its interaction with all the other particles can be calculated. Similarly, the potential energy of every other particle is also calculated. Adding them gives the net potential energy of the system. Now that the energy is know, the force acting on a particle can be calculated as:

$$F_x = \frac{\partial \phi(\vec{r})}{\partial x} \tag{1.6}$$

This expression is for a 1D case but can be easily extended for a 3D system.

This is usually the most time consuming part during MD calculations because it is an N^2 operation where N is the number of atoms. Fortunately, there exists, simplifying algorithms and techniques which can be used to reduce this dependence significantly, such as Verlet neighbors lists, so that near-linear scaling can be achieved.

1.7.3 Integration of Newtons equation of motion

Now, the Newton's equations of motion are integrated. This is done using many different algorithms, the simplest one being the Verlet algorithm. It is derived using Taylor's series expansion about the current atom position. The following expressions are obtained:

$$r(t + \Delta t) = 2r(t) - r(t - \Delta t) + \frac{f(t)}{m} \Delta t^2 + O(\Delta t^4) \quad (1.7)$$

$$v(t + \Delta t) = \frac{r(t + \Delta t) - r(t - \Delta t)}{2\Delta t} + O(\Delta t^2) \quad (1.8)$$

This expression offers the velocity of the particle at the future time step at the cost of accuracy. H

but to calculate the velocity it uses accelerations calculated from the forces on the particles. The expression for velocity now becomes:

$$v(t + \Delta t) = v(t) + \frac{a(t + \Delta t) - a(t)}{2} \Delta t + O(\Delta t^2) \quad (1.9)$$

Now, we have an expression which is second order accurate. There are many other higher order schemes such as the predictor corrector methods, but for general

purposes second-order accuracy is adequate. For details of this method and other higher order methods we refer to [20].

1.7.4 Equilibration

Equilibration is the stage where statistical fluctuations are a minimum and the sample is now ready for study. The time required for this depends on the system size, system density and mass- and thermal diffusion properties of the system. Systems with a low mass- or thermal diffusion will take longer to reach equilibrium.

1.8 Simulation bulk systems: Periodic Boundary Conditions

While we are interested in obtaining the thermodynamic properties of a macroscopic system which has millions of particles and even greater degrees of freedom, the number of atoms in a typical simulation ranges only of the order of thousands. So the problem of simulating a true macroscopic system arises. This problem is partially solved using the concept of periodic boundary conditions (P.B.Cs).

It is assumed that the system under consideration is a unit cell and an entire lattice, which is essentially has infinite copies of the unit cell, is simulated. A collection of all these copies is called an ensemble. More details on the different kinds of ensembles are discussed in the following section. Fig. 1.7 better explains the previous statement.

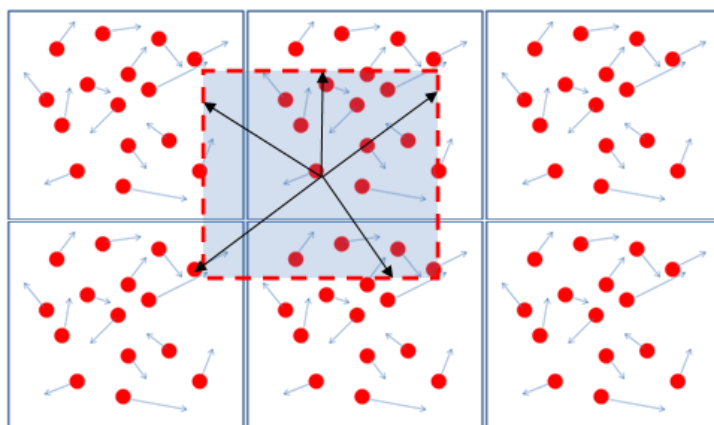


Figure 1.7: Simulation of bulk systems: Periodic Boundary Conditions

Even though the number of particles remains the same the number of interactions does not. For example, if we take long range interactions, then each particle does not see and interact with the particles in its own box but also the images of these particles in their periodic images. If these images extend in all three dimensions then the simulation approaches the limit of a bulk system.

However, a drawback of this modification is that it replaces the finite pair-wise potential energy summation with an infinite sum as there are infinite interactions. Fortunately, most of these interactions rapidly decay with distance and hence approximations can be made beyond a certain distance. Ewald's summations is an example of Coulomb's interactions. In ReaxFF, the long range interactions do not drop fast enough and hence the taper function is used.

1.9 Types of ensembles

While PBCs impose the bulk system condition, they do not govern the interactions between particles that lie in different unit cells. For this purposes different boundary conditions allow exchange of energy, particles, pressure etc depending on the setup. Based on the kind of boundary conditions, the ensembles are classified as follows:

1. Micro-canonical ensembles
2. Canonical ensembles
3. Grand canonical ensembles
4. Isothermal/Isobaric ensembles

1.9.1 Micro-canonical ensemble

The flowchart shown in Fig. 1.5 represents the micro-canonical ensemble (NVE), which in macroscopic terms is a ‘constant energy’ adiabatic simulation. This means that if the potential energy of any member of the system goes down, its kinetic energy must go up which in turn raises the temperature of the system. Hence different cells might have different temperatures. The description of the NVE ensemble is what has been described as the MD algorithm.

Even though this is relatively easy to apply, it seldom resembles experimental conditions which take place at constant temperature and pressure. This introduces the need for different ensembles.

1.9.2 Canonical ensemble

The Canonical ensemble has a constant number of atoms, volume and temperature (NVT). Hence all particles will be at thermal equilibrium. In order to achieve a desired temperature, energy is pumped in the form kinetic energy and is distributed equally over all atoms. Various algorithms are used to achieve this effect. In our simulations, the Berendsen's thermostat [21] is used. A brief description of this thermostat is given below.

1.9.2.1 Berendsen's thermostat

When the system needs to be at a specified temperature, it is done by velocity scaling using the energy correlation. We can use the Kinetic Energy-Temperature correlation as defined by Eq. 1.3; consider the following equations which represent the temperature difference:

$$\Delta T = \sum_i \frac{m(\lambda v_i)^2}{k_b T} - \sum_i \frac{m v_i^2}{k_b T} \quad (1.10)$$

$$\Delta T = (\lambda^2 - 1)T(t) \quad (1.11)$$

The velocity scaling factor λ is defined as

$$\lambda = \sqrt{\frac{T_o}{T(t)}} \quad (1.12)$$

where $T(t)$ is the current temperature of the system and T_o is the desired temperature. This form of definition has a problem in that the temperature change would be instantaneous

and hence discontinuous. To avoid this problem we scale the temperature using the thermostat constant (τ) . The temperature is now defined as follows:

$$\frac{dT}{dt} = \frac{1}{\tau(T_o - T(t))} \quad (1.13)$$

Thus the Berendsen's thermostat gives an exponential decay towards to desired temperature and τ is a coupling factor that determines the rate of decay. If the value is low, then the thermostat is strongly coupled. For a very high value ($\tau \rightarrow \infty$) , the thermostat does not function and essentially the canonical ensemble is now a micro-canonical ensemble. Thus the scaling factor for velocity becomes:

$$\lambda^2 = 1 + \frac{\delta t}{t} \left(\frac{T_o}{T \left(t - \frac{\delta t}{2} \right)} - 1 \right) \quad (1.14)$$

Other thermostats are the Anderson thermostat [22] and the Noose-Hoover thermostat [23][24].

1.9.3 Isothermal/Isobaric ensemble

The isothermal/isobaric or NPT ensemble is a constant temperature – constant pressure simulation. Here, the volume of the simulation box is changed, so as to drive the pressure of the system towards the specified pressure. The temperature thermostat is active as mentioned earlier. Thus, members of the ensemble will be at thermal and pressure equilibrium.

A constant pressure is maintained by changing the shape and dimensions of the box as required. Often, it is essential that the change in the shape of the box allow for transformation such as change in state of a crystal without creating highly stressed configurations. This problem was first tackled by Parrinello and Rahman [15][16] which is currently used strain relation of wire to thermal conductivity.

1.9.4 Grand-canonical ensemble

The grand canonical ensemble is an ensemble where members can exchange energy and particles. Hence, there will always be thermal and chemical equilibrium. This method has not been used in any of the simulations in this thesis and hence is not described in detail. It is most commonly used in simulation of adsorption studies of a gas on a solid as a function of temperature and concentration

To conclude, Molecular Dynamics can be viewed as a virtual experiment, with a very fine spatial and temporal resolution. Of course, like real life experiments, a lot of things can go wrong in a MD ‘experiment’, but it proves to be a reliable method when a well-trained force field is employed and the results are averaged over a large number of simulation runs (and/or a large number of atoms is used in the system). MD is thus a powerful tool to study the properties of materials qualitatively, which is what is intended in this project: to calculate the qualitative variation of thermal conductivity of a nanowire with increasing strain.

1.10 Types of Force fields

Scale of a simulation is an important factor that must be decided before the starting any simulation or experiment. Fig. 1.8 shows the different scale of experiments. At the very bottom of the spectrum we have Quantum Mechanics. These simulations are accurate but are limited to small system size. At the higher end we have the macroscale experiments which have direct application to real world applications but lack the ability to capture reaction time scales. Thus, in order to bridge the gap between these two disparate scales of simulation, force fields have been developed.

Force fields can be categorized in two classes – Non-reactive and reactive. Non-reactive force fields are useful in simulating molecular species and materials which are at equilibrium; but cannot simulate bond-formation/breaking correctly. Reactive force fields overcome this limitation using bond-order relations in the potential energy expressions.

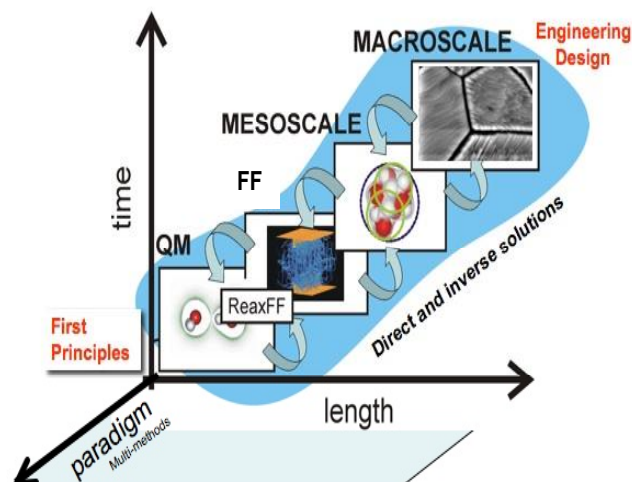


Figure 1.8: Hierarchy of different scales of simulation

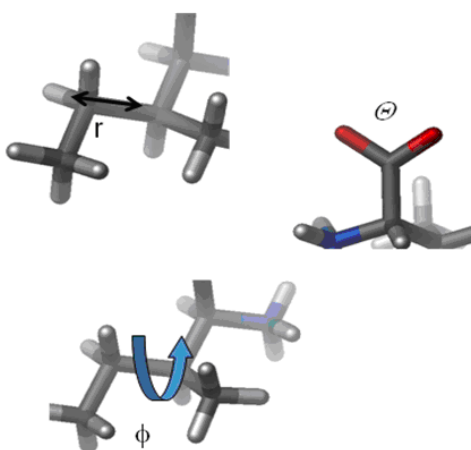


Figure 1.9: Bonded interactions (Top – bond energy, Right - Valence angle energy, Bottom – Torsion energy)

1.10.1 Non-reactive force fields

A typical energy expression for a non-reactive force field is:

$$E_{System} = E_{bond} + E_{Valence\ angle} + E_{Torsion} + E_{van\ der\ Waals} + E_{Coulombs} \quad (1.15)$$

The bond, angle and torsion energies are bonded interactions while the van der Waals and Coulomb's interaction are non-bonded interactions.

Typically; simple energy expressions for the two- and three-bonded interactions are:

$$E_{bond} = k_b(r - r_o)^2 \quad (1.16)$$

$$E_{angle} = k_v(\theta - \theta_o)^2 \quad (1.17)$$

The four-member torsion energy is:

$$E_{torsion} = V_2(1 - \cos 2\Phi) + V_3(1 + \cos 3\Phi) \quad (1.18)$$

where r , Θ and Φ are defined as shown in Fig. 1.9 . The constants that are present in each of these equations are dependent only on the equilibrium-bond properties such as equilibrium bond length and bond angle. This is the reason why non-reactive force fields are unable to simulate chemistry of reactions.

1.10.2 Reactive force field

Reactive force fields commonly use bond order terms while calculating the potential energy. Bond orders thus enable these potentials to accurately model the chemistry of molecules making them very versatile. Thus, they act as a bridge between the non-reactive force fields and quantum methods. Fig. 1.10 shows a graph differentiating between reactive and non-reactive potentials. Examples of this are the Brenner potential [18] and the ReaxFF potential [19]. Since reactive potentials involve more complex calculations they are more expensive than non-reactive force fields. Also, in order to be able to capture the high frequency bond vibration of the lighter elements such as Hydrogen, the time step needs to be smaller than 1 femto second.

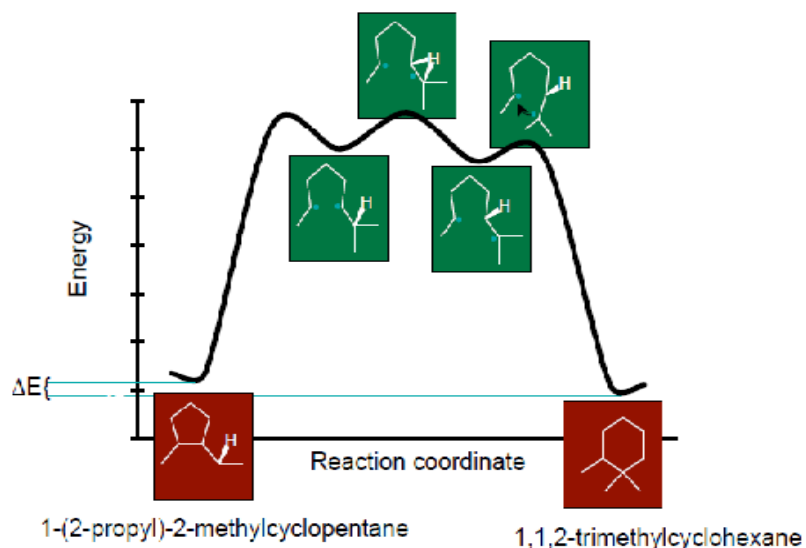


Figure 1.10: Reactive (describes brown and green states), Non-reactive force fields (describes brown states only)

1.11 ReaxFF reactive force field

ReaxFF is as a reactive force field that was developed by Adri van Duin and co-workers [19]. It uses bond order related terms to describe bonded as well as non-bonded interactions. The force field was originally developed only for hydrocarbons though it has now been successfully applied to a large number of systems such as biological molecules [25], metal oxide reactions [26], zeolites [27], organic reactions [28], thermal decomposition of polymers such as silicones and tribology of metal-metal oxide interfaces, catalytic formation of carbon nanotubes [29], storage of H₂ in Mg nanoclusters, Si/SiO₂ oxidation, crack propagation in silicon crystals [30], dissociation of H₂ on Pt surface [31].

1.11.1 Features of ReaxFF

The potential energy described by ReaxFF for any molecule is expressed as follows:

$$E_{System} = E_{bond} + E_{Valence\ angle} + E_{Torsion} + E_{van\ der\ Waals} + E_{Coulombs} \\ + E_{under\ coord} + E_{over\ coord} \quad (1.19)$$

The bonded interactions – bond, angle and torsion energy as well as van der Waals and Coulomb energies are two body terms meaning that they involve force and energy calculations between two molecules only. The Valence energy is a three body term. Torsion energy is a four body term and the over and under coordination energies are multi body terms.

Listed below are some of the key features of ReaxFF:

1. To get a smooth transition from non-bonded to single, double and triple bonded systems ReaxFF employs a bond length/bond order relationship. Bond orders are the number of bonds between atoms which can vary depending on the coordination number of the atom. They are functions of the inter-atomic distances so that the weakening of bonds with increasing bond distance is captured. Fig. 1.11 shows the bond order as a function of bond distance. Bond orders are updated every iteration. This graph arises from the following equation.

$$BO_{ij} = \exp \left[p_{bo,1} \left(\frac{r_{ij}}{r_o^\sigma} \right)^{p_{bo,2}} \right] + \exp \left[p_{bo,a} \left(\frac{r_{ij}}{r_o^\pi} \right)^{p_{bo,4}} \right] + \exp \left[p_{bo,1} \left(\frac{r_{ij}}{r_o^{\pi\pi}} \right)^{p_{bo,6}} \right] \quad (1.20)$$

2. Non-bonded interactions (van der Waals, Coulomb) are calculated between every atom pair, irrespective of connectivity. This is unlike the non-reactive force fields where non-bonded interactions are not calculated between bonded atoms. Even though it adds to computational expense; it is essential that they be calculated in reactive force fields in order to maintain the continuous nature of the energy. Excessive close-range non-bonded interactions are avoided by shielding.
3. All connectivity-dependent interactions (i.e. valence and torsion angles) are made bond-order dependent, ensuring that their energy contributions disappear upon bond dissociation.
4. ReaxFF uses a geometry-dependent charge calculation scheme that accounts for polarization effects.

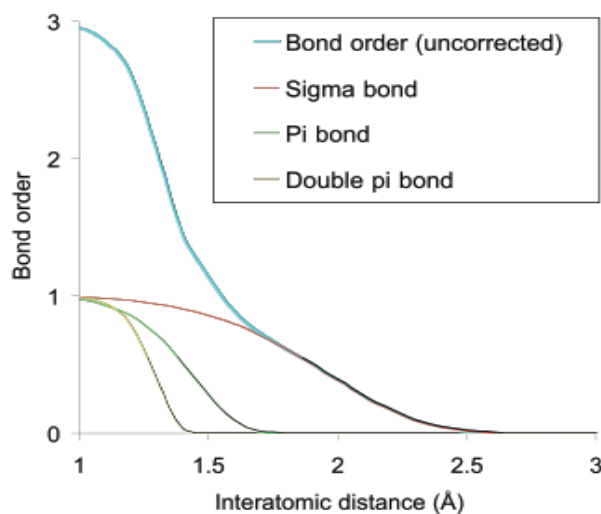


Figure 1.11: Variation of bond order with interatomic distance

Figure 1.12 shows the computational expense of ReaxFF as compared to quantum methods. Clearly the computational advantage gained by using this program justifies its use in order to speed up analyses while its versatility justifies its use of complex potential

functions. Figure 1.13 shows the periodic table containing the elements that ReaxFF is currently able to simulate.

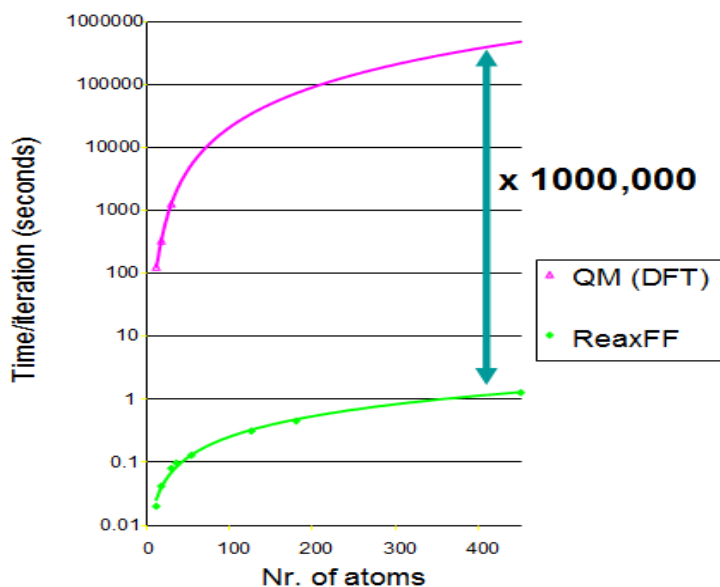


Figure 1.12: Computational expense of ReaxFF in comparison with Quantum Mechanical methods

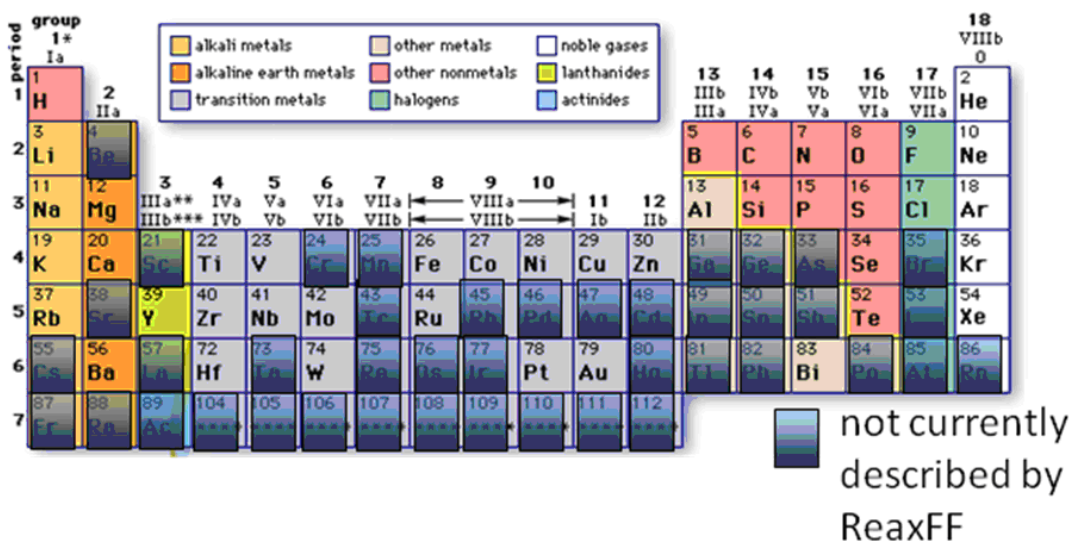


Figure 1.13: Elements currently described by ReaxFF reactive force field

1.11.2 Force field training and optimization

The general procedure in using ReaxFF is to train the force field parameters that dictate important chemical and physical properties of the elements such as energy of formation, bond breaking and polarizability. The training starts with ReaxFF using arbitrarily assigned parameters. It then creates a small perturbation in the parameter value, one which is higher and one which is lower than the initially assigned value of parameter under consideration. It now calculates the energy of the system for all three points which are then curve-fit using a parabolic fitting method. This fit will have an energy minimum. The parameter is now changed to correspond to the energy minimum of the parabola and the process is repeated again. Optimization continues until the desired energy is reached or until the user feels the force field has achieved the desired level of convergence.

1.12 Zinc Oxide

Now that a basic idea of some of the simulation methods available to study nanomaterials has been developed; the focus of this section shifts to one such material that has been gaining growing importance over the last few decades, especially since the nanotechnology initiative led by the United States. In the 1960s, Zinc Oxide played a major role in photonic devices, sensors and transducers. But with the recent advances in nanotechnology, new properties of Zinc Oxide have been discovered and its applications are ever expanding.

Study of 1D transport phenomena is one method of investigation that helps us understand size, electrical and mechanical properties of nanomaterials. Studying a low dimensional system is not only for the benefit of understanding the underlying phenomena but also for developing larger, more complex and functional systems. Zinc Oxide has emerged a key player in this study mainly because of the diverse growth morphologies like nanocombs, nanorings, nanohelices, nanowires and nanocages as shown in Fig. 1.14 [12].

Studies have shown that nanoscale Zinc Oxide has many novel properties which are not observed in its bulk state. This is mainly due to effects quantum confinement and enhanced surface area [12] [13]. We see that size of the material at the nanoscale has drastic effects on the surface area to volume ratio as seen in Fig. 1.15. Now, if we want to make a catalyst, nanomaterials would have significant advantages as it offers more surface area and hence would offer a larger surface for reactions to take place. However this effect, as we will see, is not confined to chemical properties alone and extends to mechanical, electrical and optical properties as well. The following sections describe the crystal structures of Zinc Oxide, its properties and potential applications.

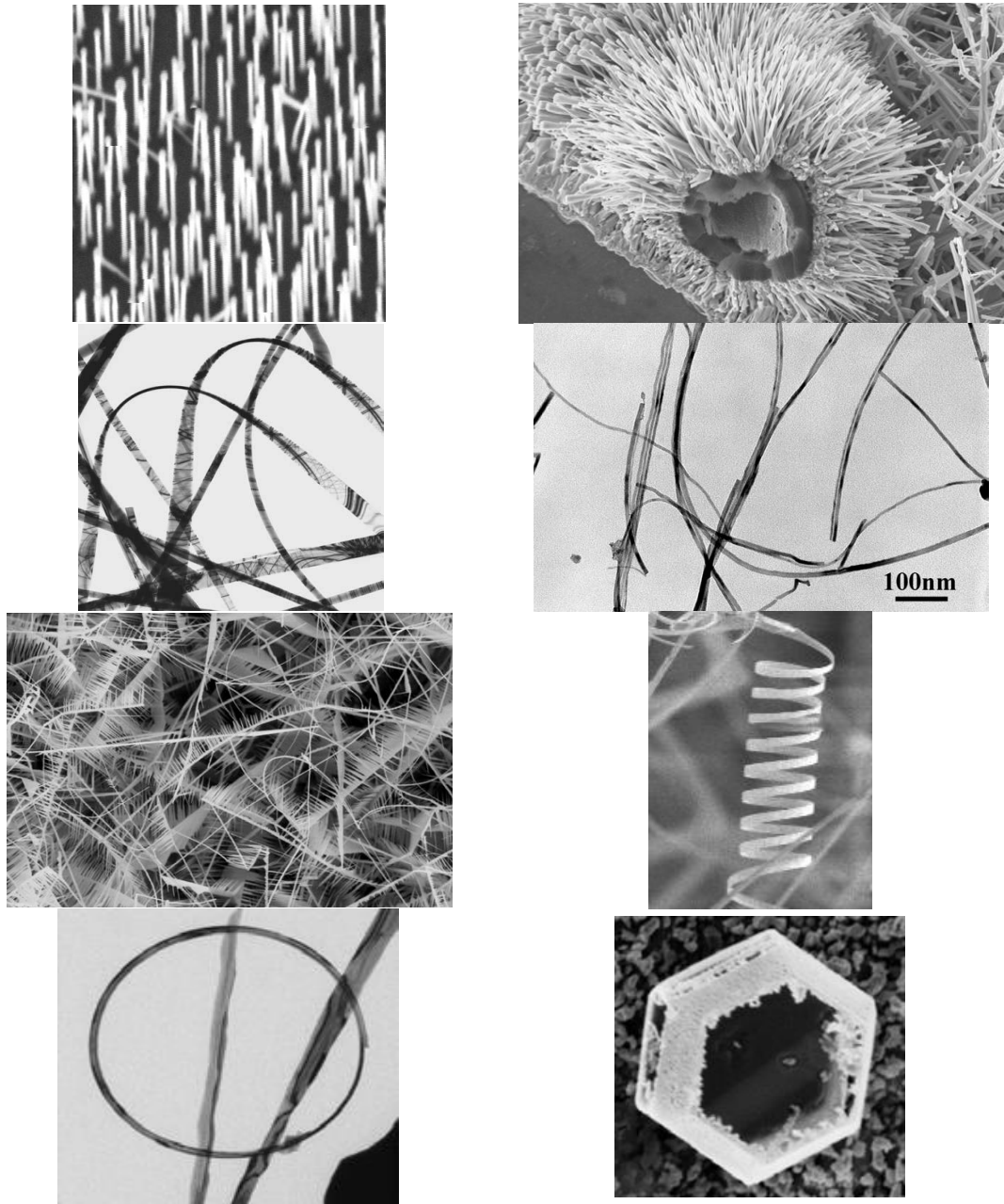


Figure 1.14: Diverse growth forms of Zinc Oxide: Nanorods/nanowires, Nanobelt, Nanocomb, Nanohelix, Nanoring, Nanocage







Full-shell Clusters		Total Number of Atoms	Surface Atoms (%)
1 Shell		13	92
2 Shells		55	76
3 Shells		147	63
4 Shells		309	52
5 Shells		561	45
7 Shells		1415	35

Figure 1.15: Surface area enhancement of materials at the nanoscale

1.12.1 Crystal structure

Zinc Oxide occurs in three crystalline forms [71] as seen in Fig. 1.16

1. Hexagonal Wurtzite
2. Cubic Zincblende and
3. Cubic rocksalt

The hexagonal structure is the most commonly occurring form and is stable at room temperature. Zincblende can be grown by using another cubic lattice as the base. Rocksalt only occurs at very high pressures. Both the hexagonal and cubic form has no

inversion symmetry. In our simulations we have focused primarily on the Wurtzite structure as this has been used in all the simulation studies. Hence, only this structure will be discussed in greater detail.

Wurtzite Zinc Oxide is largely an covalent crystal and as mentioned before, has a hexagonal closed packing with the following lattice parameters: $a = 3.296\text{\AA}$ and $c = 5.2065\text{\AA}$. All the atoms are tetrahedrally coordinated and stacked alternately as seen in Fig. 1.16 (Wurtzite). This coordination results in non-symmetry of the crystal. Another important feature is the charged surfaces. While one of the facets (0001) has a positive charge, the opposite side has a negatively charged oxygen surface. This results in a net dipole moment along the axis. An interesting feature is that, while such charged surface normally undergoes surface reconstruction, Zinc oxide remains perfectly flat and stable. This reason for its stability is yet to be explained.

1.12.2 Applications

Zinc Oxide in its nano form has many novel properties which are used for a wide range of applications. Some of them are mentioned below:

1. Photonics - It has a large band gap of 3.37eV and high excitation energy of 60meV .

This makes it an ideal material for photo diodes in the blue-UV region.

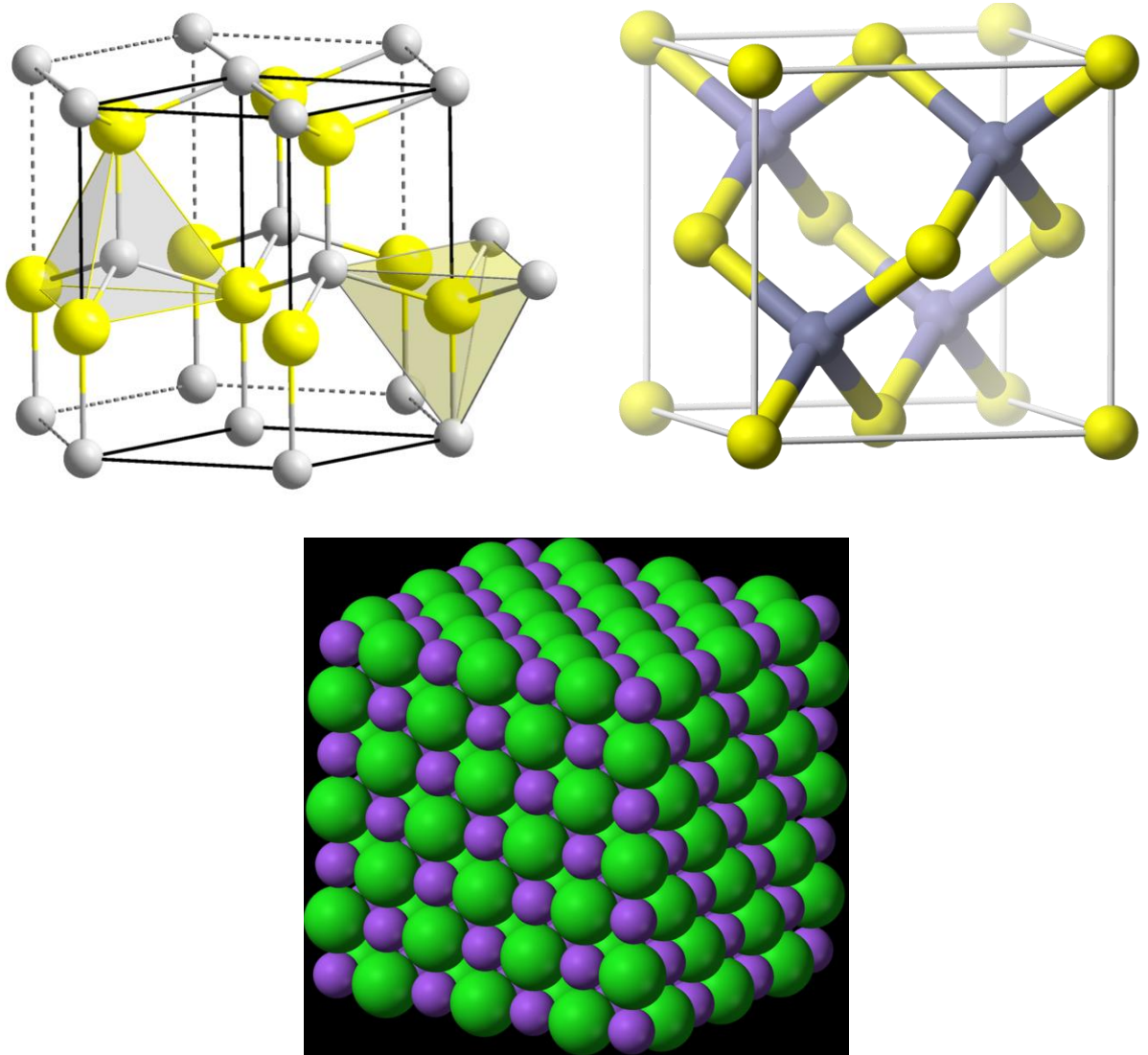


Figure 1.16: Zinc Oxide crystal structure: (Top left) Hexagonal Wurtzite, (Top right) Cubic Zinc Blende, (Bottom) Cubic Rock salt

2. Gas, chemical and biosensors – Zinc Oxide holds great promise of becoming wide spread chemical sensors with low power consumption and low costs. Their sensing is mainly based on the change in electrical conductivity due to surface chemistry reactions. This change is used to detect presence of compounds. Zinc Oxide is particularly sensitive to the presence of water as it decomposes to Zinc hydroxide.

However, a lack of stability at high temperatures over longer time frames has hampered a more universal usage.

3. Thermo-electronics – Nano materials have a lower conductivity compared to the bulk forms. This is primarily due to surface area effects. This leads to increased phonon dispersion (refer section 2.3) which inhibits thermal transport across the system. While in electronics this effect will create local hotspots, they will be very effective in thermoelectric devices.
4. Nano-resonators - Using the bending modulus, one can calculate the bending modulus of nanobelts. This property is made use of by using these belts as probes in the scanning probe microscope (SPM).
5. Piezoelectricity - Due to the strong dipole moment in the Zinc Oxide crystal, the nanowires have a piezoelectric property. On exerting a pressure along the cornering direction of the tetrahedron, the charge centers are distorted which gives rise to electric dipole. This phenomenon is widely made use of in resonators, probes in scanning probe microscopy and sensors for vibration in shop floor machines.

Chapter 2

Theory of thermal conductivity and ReaxFF

Nanotechnology is of growing importance in the field of semiconductors. Over the past decades, the size of features on integrated circuits has been decreasing rapidly and with current fabrication techniques are approaching the 10nm limit. At such small scales, they need to be efficiently cooled in order to avoid hot spots. In order to make efficient design, it is important to understand the physics behind conduction from the micrometer down to the nanometer scale. The following sections describe in brief the physics behind the phenomena.

This chapter is divided in three sections. The first section gives a general introduction to Kinetic Theory of Gases (KTG), its assumptions, implications and shortcomings and using the principles of KTG, to obtain an expression for thermal transport in nanomaterials. In the second section, we aim to understand the physics behind conduction using phonon transport theory and surface scattering. The third section is a literature review of the current research trends in Zinc Oxide thermal conductance applications.

2.1 Kinetic theory of gases

Thermodynamics deals with the properties of materials at the macroscopic scale. It has successfully described the behavior of many elements. However, it is purely

empirical science and it is not possible to derive absolute magnitudes of properties such as temperature and pressure. This is solved if we take in to account the fact that matter is not continuous but discrete and is made up of individual atoms/ molecules. The theory that is developed based on this assumption tackles it in two ways. The first is that of the KTG where classical Newtonian laws are applied to molecules. This assumption is similar to the underlying assumptions of molecular dynamics. The second is where molecules are not treated individually but applies probability theory to a very large number of atoms. This is called statistical thermodynamics. Both approaches have been fully developed and have good concurrence.

Even though many characteristics of materials could be explained using either approaches, they were derived based on the observations made on bulk materials and hence not all results were in accordance with experimental data. This led to the development of Quantum theory. KTG is discussed in the following sub sections.

2.1.1 Assumptions

The following are some of the basic assumptions of KTG:

1. Any macroscopic volume has a very large number of molecules.
2. The molecules are separated by distances much larger compared to their own dimensions.
3. They do not exert any forces on each other until they collide.

4. Collisions between molecules, between walls and molecules are perfectly elastic.
5. The distribution of molecules is isotropic.
6. The direction of molecular velocities are assumed to be uniform.

Some of the assumptions mentioned above are not always valid. For example the assumption that molecules don't interact with each other except on collision is not true. The forces are weakly attractive at long distances but strongly repulsive at close distances as has been discussed in Section 1.7.2. Another flaw is that, KTG treats atoms as points (implied in assumptions 2 and 4) and hence can fly freely, generally without colliding with any other molecule. This means that if we open a container of gas, then it would spread instantaneously throughout the room. But this is actually not the case. Instead the gas diffuses slowly across the room as it undergoes a number of collisions with the other gas molecules. This gives rise to the principle of diffusivity of a gas. In order to explain this fact, the concept of mean free path is introduced. The derivation of the mean free path is discussed below. Its importance in thermal conductivity will become apparent in future sections.

2.1.2 Mean free path

Fig. 2.1 shows the collision condition between two molecules. Since molecules are considered as rigid spheres (assumption of KTG), the collision condition for two molecules is that the distance between them should be the sum of their radii. In the figure,

the circle of radius d (which is the distance of separation) is called the sphere of exclusion. It can also be said that the collision of atoms depends only on the inter-atomic distance and does not depend on the individual molecular size or any other property. Hence let us modify the atoms in Fig. 2.1 such that one of the atoms is made very small, called the ‘bullet’, and the other atom made very large, called the ‘target’. Now consider a cuboid of side L and thickness Δx containing some target molecules which are fixed as shown in figure 15. Let a number of bullet molecules have trajectories passing through this cuboid. Since the bullets are much smaller, most of them will pass through. Let us define a ratio based on the number of collisions (ΔN) and the original number of atoms (N). This should be equal to the ratio of the target area to the total area.

$$\frac{\Delta N}{N} = \frac{\text{Target area}}{\text{Total area}} \quad (2.1)$$

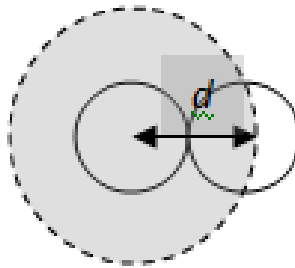


Figure 2.1 Sphere of exclusion: Minimum collision distance between atoms determines mean free path

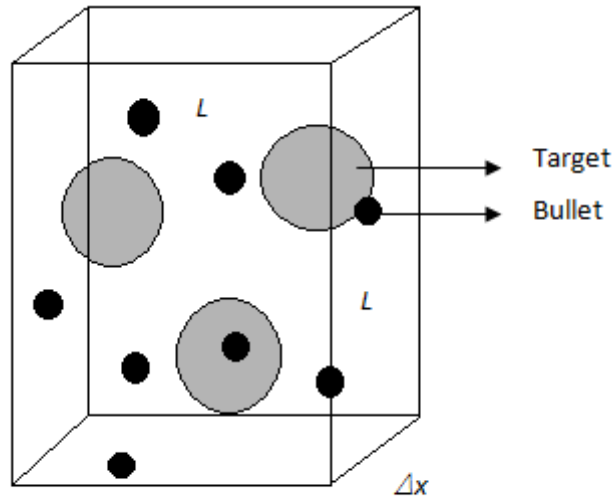


Figure 2.2: Survival equation: Number of smaller bullet molecules that do not collide with larger target molecules

The target area is nothing but the sum of the projected area of cross-section of all the molecules. If n is the number of molecules per unit volume and d the radius of the sphere of exclusion, then the target area is given as

$$n\pi d^2 L^2 \Delta x \quad (2.2)$$

If we write πd^2 as the microscopic collision cross-section – σ , then Eq. 2.1 becomes

$$\frac{\Delta N}{N} = \frac{n\sigma L^2 \Delta x}{L^2} = n\sigma \Delta x \quad (2.3)$$

Here $n\sigma$ is called the macroscopic collision cross section. If we choose to integrate Eq. 2.3, we get the following expression:

$$N = N_o \exp(-n\sigma x) \quad (2.4)$$

Where N is the number of molecules that have not yet collided and N_o is the original number of molecules. This is known as the survival equation. Substituting Eq. 2.4 in Eq. 2.3, we get:

$$\Delta N = N_o n \sigma \exp(-n\sigma x) \Delta x \quad (2.5)$$

In this equation, ΔN represents the decrease in the number of molecules N due to collision having after having travelled a distance Δx .. The mean free path is defined as the average distance that a molecule will travel before it makes a collision. Therefore, averaging the above distance travelled between collisions will give us the mean free path.

$$l = \frac{\sum x \sum \Delta N}{N_o} = n\sigma \int_0^{\infty} x \exp(-n\sigma x) dx = \frac{1}{n\sigma} \quad (2.6)$$

More accurate expressions for the mean free path can be obtained by considering both the target and bullet molecules as mobile and keeping the Maxwell Boltzmann velocity distribution we obtain:

$$l = \frac{0.707}{n\sigma} \quad (2.7)$$

2.1.3 Thermal conductivity

Consider two plates at different temperatures so that there is a thermal gradient normal to the surface within the gas. The thermal conductivity (κ) is defined by:

$$H = -\kappa \frac{\partial T}{\partial y} \quad (2.8)$$

From a molecular viewpoint, the thermal transfer is due to the flux of kinetic energy from the high temperature to the low temperature surface. For a bulk material, the total kinetic energy per mole is defined as its internal energy c_v . Thus the internal energy of a single molecule (c_v^*) is obtained by dividing the c_v by the Avogadro number (N_A). From fundamental principles of KTG, it can be derived that the average distance a molecule makes a collision before crossing surface is two-third its mean free path.

If the lower and hotter surface is at temperature T_o and we are interested in finding the temperature of the surface above that, then by conservation of energy we have:

$$c_v^* T = c_v \left(T_o - \frac{2}{3} l \frac{\partial T}{\partial y} \right) \quad (2.9)$$

Thus heat currents across the layers just above and below the surface with temperature T_o are given as:

$$\vec{H} = \frac{1}{4} n c_v^* \bar{v} \left(T_o - \frac{2}{3} l \frac{\partial T}{\partial y} \right) \quad (2.10)$$

$$\vec{H} = \frac{1}{4} n c_v^* \bar{v} \left(T_o - \frac{2}{3} l \frac{\partial T}{\partial y} \right) \quad (2.11)$$

Therefore the net heat current is:

$$H = -\frac{1}{3}nC_v^*\bar{v}\frac{\partial T}{\partial y} \quad (2.12)$$

Thus the thermal conductivity is defined as:

$$\kappa = \frac{1}{3}nC_v^*\bar{v} \quad (2.13)$$

This derivation has been derived based on the simplifying assumptions of KTG. However number of other factors like phonon-phonon interaction, phonon-electron interaction and phonon scattering modify the variation of thermal conductivity in several ways. This is the topic of discussion in the sections to follow.

2.2 Phonon theory

2.2.1 Specific heat of solids

Atoms in solids are held together by inter-atomic forces which are strong enough to prevent them from moving far away from their equilibrium positions. Thus they are only allowed to vibrate about these equilibrium positions. Thus Einstein proposed a model using harmonic oscillators with quantized energy levels in order to obtain specific heat as a function of temperature. However this model also failed because it under-predicts specific heats at intermediate temperatures. This was finally rectified in the Debye model. Here, instead of taking atoms as independent oscillators, inter-atomic forces causes the atoms to vibrate as a group of oscillators, much a group of objects

vibrating when inter connected with springs. The Debye model defines an upper limit for the frequency of vibration which is determined by the maximum number of degrees of freedom. This is a plausible argument as the smallest wavelength should be of the order of the lattice constants. Using this, we define the Debye temperature:

$$T_D = \frac{h\nu_m}{k_B} \quad (2.14)$$

Where, ν_m is the maximum frequency, k_B is the Boltzmann constant and h is the Planck's constant. This approach produced results that matched experimental data with reasonable accuracy for a large temperature range. The expression for specific heat in nanocrystals is:

$$C_v = a_1 T^2 + a_2 \frac{T^2}{L} + a_3 \frac{T}{L^2} \quad (2.15)$$

where L is the side of the crystal.

2.2.2 Phonon scattering

Oscillations of the atoms give rise to waves in the solid similar to sound waves. They can be of two kinds- longitudinal and transverse waves. A quanta of these waves is called a phonon. The phonons are characterized by their frequency and have an upper limit which is limited to the wavelength corresponding to twice the equilibrium distance between the atoms. Another important feature is that phonons need not be conserved just like in waves. Three-phonon and four-phonon theories have been developed based on this principle and will be discussed in more detail towards the end of the section.

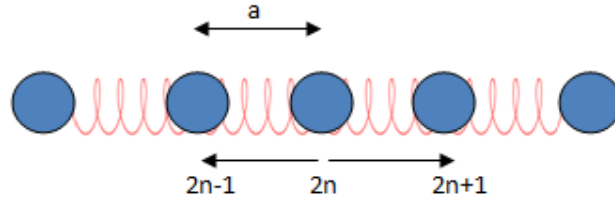


Figure 2.3: 1D chain of atoms exhibiting vibrational characteristics

Consider a 1D chain of atoms linked with each other by springs of spring constant k as shown in the Fig. 2.3. ' a ' is the relative displacement $(2n-1, 2n+1)$ of an atom from its equilibrium position $(2n)$. The relative displacement can then be governed by the wave equation. In order to simplify things it is generally assumed that the every atom is affected only by its immediate neighbor. The equation is as follows:

$$m \frac{d^2x}{dt^2} = K(x_{2n-1} - x_{2n} + x_{2n+1}) \quad (2.16)$$

Where, K is the spring constant, m the mass of the atom and x_i the position of the atom in the three positions indicated with x_{2n} being the equilibrium position. Eq. 2.16 being quadratic in nature has two roots. This gives rise to two different types of phonons – Optical phonon and acoustic phonon. Optical phonons are of higher frequency and energy. They are called so because they are excited by infrared light in ionic solids. Acoustic branch are low frequency phonons. At this stage we define another useful parameter, the phonon group velocity. It is the velocity with which the overall shape of the wave propagates and is defined as follows:

$$v_g = \frac{d\omega}{dk} \quad (2.17)$$

The group velocity of optical phonons is usually very small and hence they do not contribute to thermal transport. However, they can impede thermal transport by interference with acoustic phonons. This effect is more prominent at higher temperatures which are why thermal conductivity decreases as temperature increases. Another important parameter in relation to phonons is the crystal momentum. Its significance in phonon scattering is explained in the three-phonon scattering process below. According to wave-particle duality, a phonon must have a physical momentum. However, when they move through the lattice they do not carry any physical momentum. This becomes apparent only when they interact with electrons or photons. This momentum is called the crystal momentum. Just like energy, this momentum is also conserved as long as there are no inelastic phonon-phonon interactions.

An important phenomenon is scattering of phonons at boundaries. This occurs if the mean free path of the phonons is larger than the characteristic length of the material. In crystals, the characteristic length is many orders of magnitude larger than the wavelength of phonons. However, in nanomaterials, the mean free path of phonons is about 10 to 100nm and hence suffers from boundary scattering. This in turn reduces the thermal transport due to loss of energy. It is not only at boundaries that phonons are scattered but they also interact with defects in the material. These defects can be of many forms such as holes, grain boundaries, impurities and vacancies. Scattering depends on the wavelength of the phonons and not on the temperature. At low temperatures, the system has a low degree of freedom and hence the wavelength of the phonons is large and comparable to the size of defects corresponding to the low energy. As the

temperature increases, the thermal storage capacity of the system, i.e. c_v increases. Phonon-phonon interactions still do not contribute too much to the thermal resistance. Hence, the thermal conductivity of the system increases. As we approach the Debye temperature, the phonon-phonon interactions become dominant and their contribution to the thermal resistance goes up with further increase in temperature. However, once all the vibrational modes have been excited, the c_v value does not increase concomitantly. Hence, the thermal conductivity decreases beyond this point.

The phenomenon of thermal scattering is explained by the three-phonon scattering theory. There are two possibilities by which the phonon interaction can take place: either two phonons can combine to form a single phonon or a single phonon can break into two different phonons. If the crystal momentum is conserved on the process, then it is called the Normal process or the N-process. This process does not alter the net energy transfer and hence does not contribute to any thermal resistance. The Umklapp or U process involves loss of momentum and hence introduces thermal resistance thus reducing thermal conductivity. Of course, processes involving more number of phonons are possible; however at room temperature the three phonon process has the greatest probability.

2.3 Literature review of thermal transport in Zinc Oxide

Zinc Oxide is an active area of research due to the range of interesting properties it possesses as described in section. This section covers the recent research advancement

in Zinc Oxide. Starting with general synthesis procedures and newly developed techniques, the section quickly zooms into thermal conductivity work carried out on Zinc Oxide. After discussing the general techniques used to calculate thermal conductivity, the novel method developed is presented. Following this, a brief introduction to grain boundaries and the studies done on Zinc Oxide grain boundaries are discussed. Research work on effect of strain on thermal conductivity is also presented.

2.3.1 Synthesis

Synthesis of Zinc Oxide nanowires is a widely researched field. Evaporation and condensation in gas phase are one of the popular methods as the results obtained from these methods are high quality products [37]. A detailed explanation is available in the review by Zhong [12]. However, this method requires expensive substrates and high temperatures which increase the cost of synthesis. Growing them in aqueous media is a suitable alternative [38]. Using pre-aligned Zinc Oxide [39] and pre-seeding it with a substrate such as glass or silicon, in medium Zinc acetate in a hydroxyl rich environment, one can obtain high quality Zinc Oxide nanowires. Laser pulse deposition is another promising method [40][41]. Other methods include sol-gel [42], chemical vapor deposition [43], thermal [65] and hydrothermal growth [44].

2.3.2 Thermal conductivity

Among the different physical attributes of a substance, thermal conductivity is a very important and interesting design property. Although this is a bulk property, we start by analyzing it as a one dimensional thermal transport problem. This helps us understand the underlying phenomena in heat transfer which can then be extended to larger scales as needed during design [46]. Nano-thermal conductivity of a large number of materials like GaN, SiC, UO₂ and ZnO has been studied in their forms for various applications. Zinc Oxide with its numerous morphologies has been one of the widely studied materials.

Measurement of thermal conductivity of bulk Zinc Oxide was performed by Pollack et.al [46] for different surface treatments. The average thermal conductivity thus measured is found to be between 100-120 W/m-K. Similar results have been obtained by Florescu et.al [47]. Olorunyolemi et.al [48] performed similar thermal conductivity measurements for particulate Zinc Oxide ranging from micro- to nano- size. It was seen that thermal conductivity increased as particle size decreased. The value of conductivity is found to be 0.75 W/m-K for micro- and 1.16 W/m-K for nano sintered powder. Also, the heating the powder showed a decreased thermal conductivity as expected. This concurs with the phonon theory Umklapp process. The striking feature is that the thermal conductivity of nano-Zinc Oxide is about 10 times smaller than that of bulk Zinc Oxide. Another observable trend is the decreasing thermal conduction with increase in temperature.

Study of the effect of the nanowire size on conductivity has been performed by many researchers. Kulkarni and Zhou [49] performed simulation with three different sizes of nanobelts. They found that as surface-to-volume ratio increases, the thermal conductivity decreases due to increased surface scattering. They also found that thermal conductivity decreases with increasing temperature due to increased three-phonon, four-phonon interaction and optical phonon interference. In another work by the same authors [50], they studied the effect of strain on thermal conductivity. They found that as thermal conductivity increases by as much as 20-28% with tensile strain until failure. Study of crystals with defects is a focus area for research as it is difficult to get a perfect crystal structure. Moreover, it is always possible that the structure of the crystal can change during its use causing its properties to use. Hence, defects like vacancies and grain boundaries have been studied quite extensively. Grain-boundary scattering in nanocrystalline thin films has been studied by Feng et.al [54]. They observed severe electron-surface scattering which drastically affects the thermal conductivity. Though the electron scattering does not contribute to conductivity in Zinc Oxide, the underlying physics is the same in both cases. An interesting study by Kun Yan and Ai-Kah Soh [55] compares the thermal relaxation time required by a sample with and without grain boundary. They found that because of thermal impedance from the grain boundary, the relaxation time, which is the time needed for the system to reach thermal equilibrium, required is 20% longer than if there was no grain boundary. While relaxation time is one form of grain boundary characterization, some authors prefer using Kapitza conductance/resistance [56][57]. Kapitza resistance is defined as:

$$J = \sigma_k \Delta T \quad (2.18)$$

Where J is the heat current, ΔT is the temperature difference at the grain boundary and σ_k is the Kapitza conductance. Inverse of the conductance will give resistance. Fundamentals of the processes of grain boundary scattering have been well-addressed by Maiti *et.al.*[57].

All of the above mentioned simulations used only the Green-Kubo method [52] in order to obtain the thermal conductivity. A brief description of this method is given below. Green-Kubo method is a equilibrium MD method that uses fluctuations in thermal current in order to calculate the thermal conductivity. The thermal and mechanical process that we see in everyday life have a very interesting property that flux vector shares a linear relationship with the field causing the flux and low to moderate gradients. Some examples are the Ohms law which related current with the applied voltage with the constant conductance which is the inverse of resistance. The shear stress is related to velocity gradient by the coefficient of viscosity. Similarly, the thermal current is related to the thermal gradient by the thermal conductivity. Thus, in general we can write:

$$J = L(0)F_e \quad (2.19)$$

Where, J is the flux, F_e is the field and $L(0)$; the linear transport coefficient. In the 1950s, M.S.Green and R Kubo found the exact relation for the linear transport coefficient at any temperature and density.

$$L(0) = \frac{V}{k_b T} \int_0^\infty ds \langle J(0)J(t) \rangle_{F_e=0} \quad (2.20)$$

Where, V is the volume of the system, T the system temperature, J the thermal current at some time t . Using the above relation, one can find the thermal conductivity of any system.

This method is very reliable and produces results with good accuracy. However, the main drawback of using this method is need to average the auto-correlation function over a very large time period usually in the order of nanoseconds. An alternative method is proposed in the work by Schilling *et.al.*[52] with Silicon crystals. Using non-equilibrium simulations by applying a temperature gradient, they calculate the thermal conductivity using Fourier's law of heat conduction.

Their results match closely with those obtained from the conventional Green-Kubo method. This method requires much shorter simulation time. But, the use of very high temperature gradients introduces non-linearity to the temperature profile. Boundary scattering of phonons is also high as the source and sink coincide with the edges of the wire. These are rectified using statistical averaging thermal transport across the source-sink has reached an equilibrium.

Another interesting method of calculating thermal conductivity is the experimental work done by Righini *et.al.*[53]. A specimen is heated up to a temperature of 1000°C. The temperatures at different points on the sample are then recorded using a

high-speed scanning pyrometer. Using the temperature profiles obtained at different points in time, it is then possible to calculate the thermal conductivity using the thermal transport equation. This method has been replicated using molecular dynamics [55]. A detailed explanation of this method has been provided in chapter 3.

2.3.3 Zinc Oxide force fields

A wide cache of literature exists for Zinc Oxide. Numerous studies using *ab-initio* quantum methods and Density Functional Theory (DFT) of Zinc Oxide have been published [59][60][61]. Results from quantum calculations using hybrid quantum methods like B3LYP have been published [61][62]. However like all quantum methods, they are slow and are limited in application to small system.

Force field development of Zinc Oxide for ReaxFF is presented in the work by Raymand et.al. [58]. The force field training set consisted of Quantum Mechanical (QM) calculations of the following structures:

1. Four crystalline forms of Zinc Oxide, namely: Wurtzite, Zincblende, Rocksalt and Caesium Chloride structure. Potential energy curves were calculated for each of the polymorphs and used in the ReaxFF training set.
2. Five ZnO surface systems were studied. The surface energy, surface relaxation and surface rumpling were calculated and used in training set.
3. Equations of state for Zinc metal: hexagonal close packing (h.c.p), face centered cubic (f.c.c), body centered cubic (b.c.c), simple cubic (s.c).

4. Equation of state and geometry optimizations for two Zinc hydroxide clusters and $O(\text{ZnOH})_2$

Chapter 3

Thermal conductivity simulations and results of Zinc Oxide

The simulations carried out to calculate the thermal conductivity are described in this chapter. The first section describes the Steady-State Non-Equilibrium Molecular Dynamics (SS-NEMD) methodology and the details of the simulation and case studies. This is followed by the Transient Non-Equilibrium Molecular Dynamics (T-NEMD) methodology. The theory as explained in [53] is described in detail and its modifications to the current simulations are specified. The sintering process of Zinc Oxide is discussed in section with the application of the NVE method. At the end of every section, the related results are discussed.

3.1 Steady State Non-Equilibrium method (SS-NEMD)

This direct method of measurement is based on the simple application of the Fourier law of heat conduction, given by

$$J = kA_r \frac{\partial T}{\partial x} \quad (3.1)$$

Where, J (W) is the thermal current, k (W/m-K) is the thermal conductivity, A_r (m^2) is the cross-sectional area of the wire and $\partial T/\partial x$ (K/m) represents the thermal gradient.

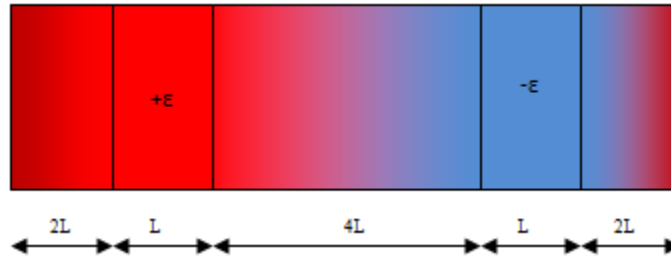


Figure 3.1: Schematic representation of the SS-NEMD method (Red represents the hotter regions, blue shows the colder regions)

The Berendsen's thermostat controls the kinetic energy of the system. The thermostat can either be strongly or weakly coupled to the system by using a low or high damping constant respectively. A Velocity-Verlet algorithm is used to integrate the equations of motion. The time step used is 0.25fs.

Fig. 3.1 shows a schematic representation of the SS-NEMD system. The temperature decreases from red to blue. Initially, the system is energy minimized and then pre-equilibrated to an average temperature, between the hottest and coldest temperatures to which the system will be set. Then two regions are defined within the system as described by Schelling *et.al.* [52] (the regions of length L). The width of the two regions is chosen in the ratio as shown in Fig. 3.1. These are strongly coupled with the thermostat (100.00 fs) and are heated/ cooled to the assigned temperatures. The rest of the system is coupled weakly (100000.00 fs) with the thermostat. This allows a temperature gradient to develop between the hot-cold regions. Once the assigned temperatures are reached, the simulation is continued for a longer period of time until an equilibrium gradient is attained. A system is said to have attained equilibrium if the fluctuations in the total system energy is at minimum. Theoretically this would take a very long time as statistical fluctuations associated with the MD simulation do not permit

the system to reach true equilibrium. For most cases, a minimum equilibration time of 20ps is found to be sufficient. The average energy pumped in/ extracted out at every time step ($\bar{\epsilon}$) is given by

$$\bar{\epsilon} = \frac{\sum_i^N \epsilon_i}{N} \quad (3.2)$$

where N , is the total number of iterations and ϵ_i is the energy pumped in at each time step.

Ideally, at equilibrium, the energy extracted should equal to the energy added. But this would take very long time as mentioned before. Thus, $|\bar{\epsilon}_{heat} - \bar{\epsilon}_{cool}| = 0.005 \frac{Kcal}{mol}$ is used as the criteria for determining equilibrium. In accordance with the limits placed on ($\bar{\epsilon}/A$) in [52], the calculated values are found to be near $3.84 \times 10^{-3} \text{ J/m}^2$. Thus; deviations in conductivity calculated from Fourier's law are negligible. Further details of the simulation are given in the following sections.

The temperature profile that develops at the end of equilibration can be found by averaging the temperature of each atom, at every time step, over all the iterations. This is given as

$$\bar{T} = \left(\frac{\sum_i^N T_i}{N} \right)_n \quad (3.3)$$

Where, T is the temperature (K), n represents the atom number and N represents the total number of iterations. A plot of the temperature profile obtained is shown in Fig. 3.2. The marked region, between the low and high temperature zones, is almost linear. To verify

the linearity, three temperature regions within this zone are chosen and linear fits are made. One is the entire marked region, second is the first half of the marked region and third is the second half of the same. Also, in order to ensure that the non-linear effects associated with the source/sink do not appear in the linear fits, the slopes were measured at a distance at least $5A$ away from these regions.

Fig. 3.2 shows linear fits of the profile chosen from the three regions in figure Fig. 3.1. As shown; the slopes are within $\pm 10\%$ of each other. Thus, the linear gradient shows that the Fourier's law of conduction can be applied at the nanoscale. Since the value of the conductivity calculated depends on the value of thermal gradient, the variance in the slope measured in the three temperature regions of the marked zone can be seen as a direct measure of the error in thermal conductivity. Thus, the error is presented as the standard deviation of conductivity obtained from each of these three slopes. Finally, the thermal conductivity can be calculated as follows:

$$k = \frac{\bar{\varepsilon}}{2A_r t_s N_A} \frac{1}{\frac{\partial T}{\partial x}} \quad (3.4)$$

Here t_s (sec) is the time step, n is the number of atoms in the heating/ cooling zone and N_A represents the Avogadro number.

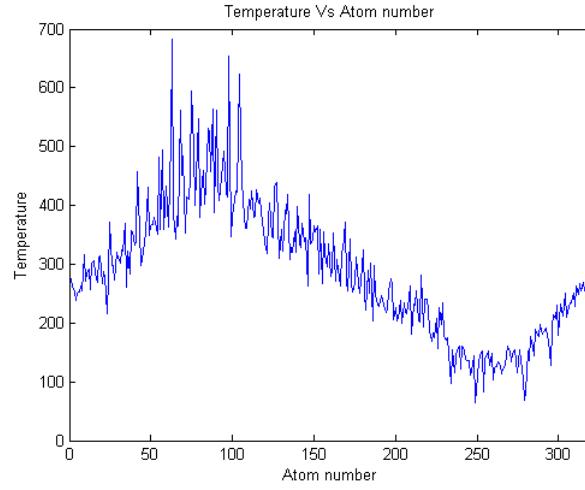


Figure 3.2: Temperature profile obtained from SS-NEMD analysis, the marked region represents the temperature profile that is used for analysis

3.2 Transient Non-Equilibrium method (T-NEMD)

This method is based on a technique that is more commonly used in macroscopic experiments as described by Righini *et.al* [53]. Application of this method to an MD environment is a new approach and to the best of our knowledge has not been tried before. Below is a description of this method.

The thermal transport equation in Cartesian form is given as Eq. 3.5

$$\frac{\partial}{\partial x} \left(k \frac{\partial T}{\partial x} \right) + \dot{g} = \rho C_p \frac{\partial T}{\partial t} \quad (3.5)$$

where ρ is the density (kg/m^3), \dot{g} is the rate of internal/ external heat generation (W/m^3) and C_p is the specific heat at constant pressure (KJ/kg-K). $\partial T/\partial x$ and $\partial T/\partial t$ represent the spatial and temporal derivatives of temperature respectively.

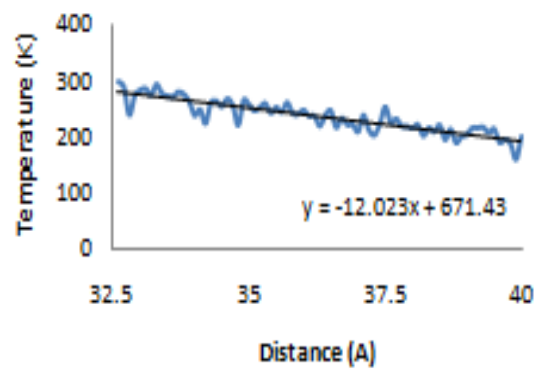
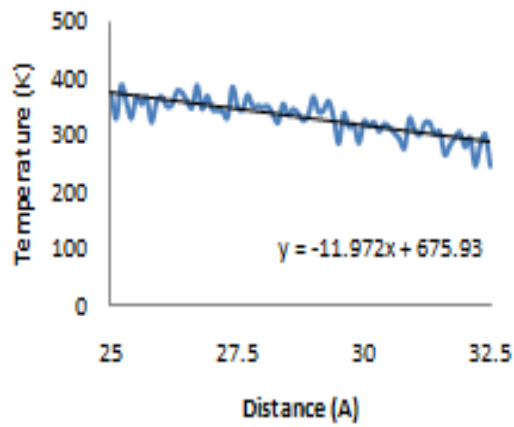
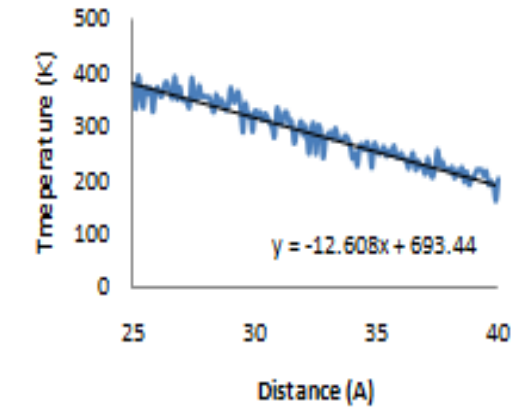


Figure 3.3: Linear curve fit for temperature zone 1(top), zone 2(center), zone 3 (bottom) obtained from SS-NEMD analysis

The simulation method is as follows. As in the SS-NEMD method, the system is energy minimized and pre-equilibrated to a specified temperature. Then a single region is defined and strongly coupled with the thermostat (100.00 fs) while the rest of the system is weakly coupled (100000.00 fs). The shape and size of the region depends on the periodicity of the system. For a one dimensional case, the region is simply a slab of certain thickness while for a two-dimensional case; it is a cylinder. A three-dimensional analysis requires a spherical region defined in the center of the system. Diagrams of the models described above are shown in Fig. 3.4.

The defined region is then heated to a high temperature. This results in a thermal gradient across the system. Then; the thermostats are switched off and the system cools naturally in a NVE type ensemble. The cooling continues until the entire system reaches an equilibrium temperature. The average simulation time needed for the system to reach equilibrium depends directly on the conductivity of the material and the temperature to which the system is heated. It typically takes 10-13ps (for a time step of 0.25fs) for the systems.

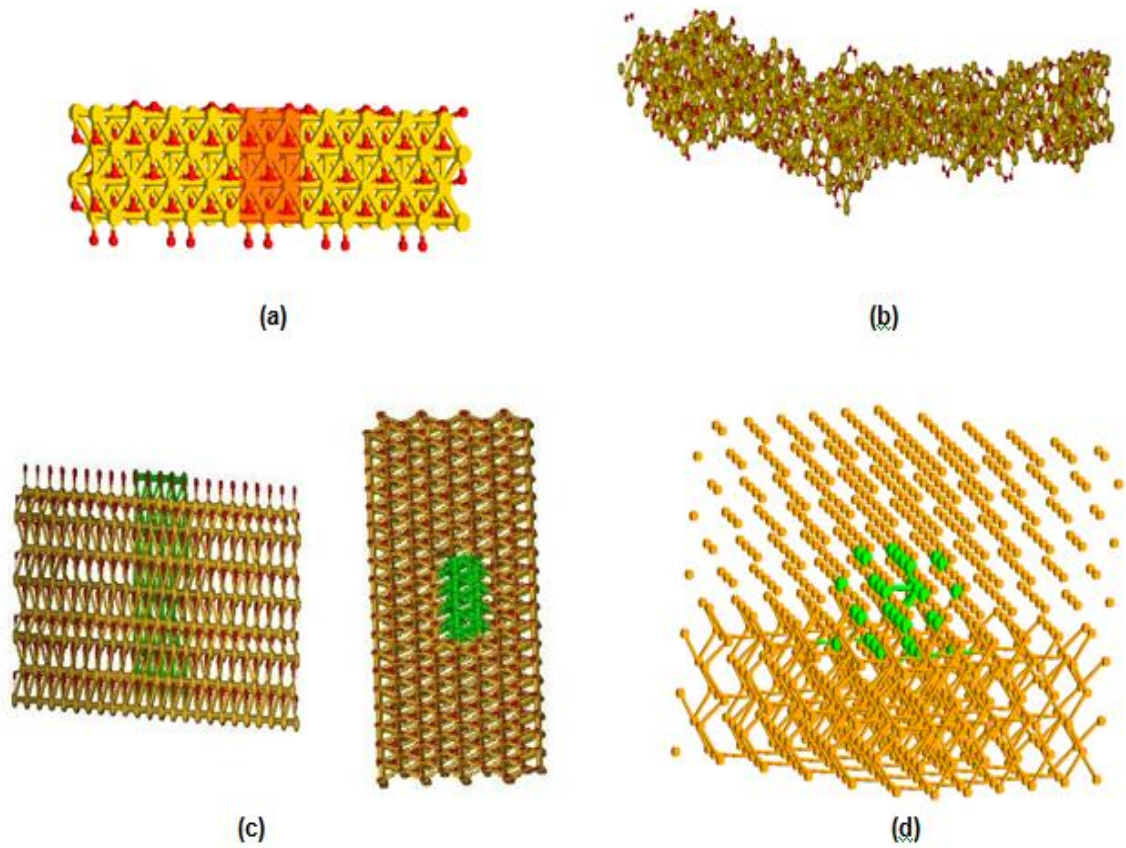


Figure 3.4: Systems used in T-NEMD method

- (a) Crystalline Zinc Oxide, 1D periodic along length, Red zone represents a slab that heats the system
- (b) Amorphous Zinc Oxide, 1 D periodic along length, Heating is similar to the crystalline system
- (c) Crystalline Zinc Oxide, 2D periodic, Green zone represents a cylinder that is heated
- (d) Solid argon crystal, 3D periodic, Green zone represents a spherical region that is heated

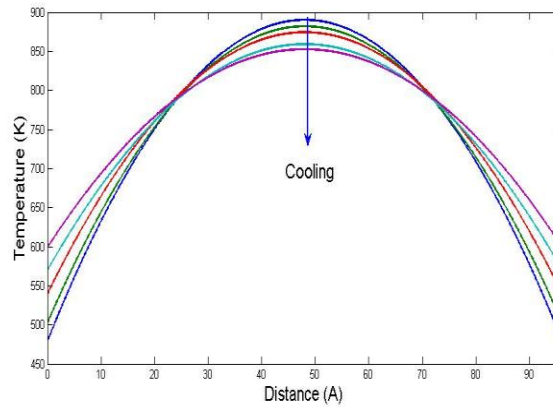


Figure 3.5: Temperature profile obtained on curve fitting MD data, each profile represents the temperature distributions at different times.

Once equilibrium is attained, the temperature profiles are derived from the cooling simulation. A block averaging technique is used to calculate the temperature of the system at different times. Averaging is done as defined by Eq. 3.3. In general, each block contains temperature information averaged from a simulation time of 2.5ps. Thus we obtain five to six temperature profiles depending on the equilibration time. Then, symmetry is forced in to the system by averaging the temperatures of all the atoms that were at the same distance from a chosen central atom. This approximation is justified as; in reality we cannot have unequal heat fluxes across the boundary of the hot zone since the material is isotropic. These temperatures obtained by averaging are subsequently curve-fitted to a low order polynomial, using the least squares method to obtain temperature profiles at different times. Fig. 3.5 shows the temperature profile obtained using the method described above.

We now assume the thermal conductivity (κ) as a second order polynomial of temperature which is represented as:

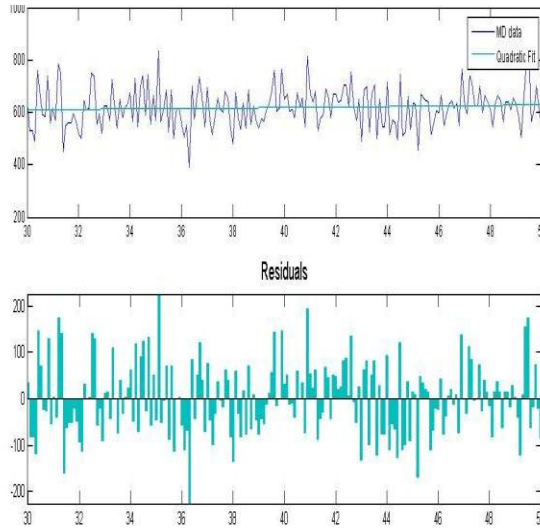


Figure 3.6: Goodness of model for MD data

(a) Top – Temperature (K) Vs Distance (A)

(b) Bottom – Residuals

$$k(T) = aT^2 + bT + c \quad (3.6)$$

By substituting expression Eq. 3.6 in Eq. 3.5 and $\dot{g} = 0 \text{ W/m}^3$, we get

$$I \quad a \frac{\partial^2 T}{\partial x^2} + b \left[T \frac{\partial^2 T}{\partial x^2} + \left(\frac{\partial T}{\partial x} \right)^2 \right] + c \left[T^2 \frac{\partial^2 T}{\partial x^2} + 2T \left(\frac{\partial T}{\partial x} \right)^2 \right] = \rho C \frac{\partial T}{\partial t} \quad (3.7)$$

In the above equation, the time and space derivatives of temperatures can be easily evaluated at different points at every time step as the temperature distributions are known from the data in Fig. 3.5. Space derivatives have been evaluated based on the quadratic fits while time derivatives have been approximated as being first-order finite difference. Refer to Fig. 3.6(a) and Fig. 3.6(b). Fig. 3.6(a) plots temperature (K) Vs

distance (A) for the MD data and the obtained quadratic fit. Fig. 3.6(b) shows the corresponding residuals. As we can see the random distribution of the residuals indicates the fit is a good model for the data. The typical R^2 values for the fit are ~ 0.55 . This value can be improved using larger systems. Thus the only unknowns are the coefficients a , b and c . Choosing points based on the recommendations in [53], we can generate a system of linear equations which can be solved using the over-determined least squares method. The precautions mentioned in [53] are meticulously followed.

Finally by substituting the values of a , b , c in Eq. 3.6; the thermal conductivity of the material at different temperatures can be determined.

While the method mentioned above works well for a one dimensional case, the approach is slightly modified so as to reduce the system from a two-/three- dimensional case back to a one-dimensional system. The Eq. 3.5 is thus modified to its cylindrical form for two-dimensional case which is given as

$$\frac{1}{r} \frac{\partial}{\partial r} \left(kr \frac{\partial T}{\partial r} \right) = \rho C_p \frac{\partial T}{\partial t} \quad (3.8)$$

and for the three-dimensional case, a spherical form is used.

$$\frac{1}{r^2} \frac{\partial}{\partial r} \left(kr^2 \frac{\partial T}{\partial r} \right) = \rho C_p \frac{\partial T}{\partial t} \quad (3.9)$$

3.3 Thermal conductivity simulations

3.3.1 Solid Argon simulations

The Morse potential used in our molecular dynamics calculations is described by:

$$V(r) = D_e(1 - ae^{a(r_e-r)})^2 \quad (3.10)$$

Where, D_e is the dissociation energy and controls the depth of the potential well, 'a' controls the width of the potential well, r_e is the equilibrium distance and r is the distance between the atoms. The values used are: $D_e = 0.32$ Kcal/mol, $a = 12\text{\AA}^{-1}$ and $r_e = 1.92$ \AA. The dissociation energy for an fcc lattice obtained using these parameters is -1.54 Kcal/mol which compares well with the -1.52Kcal/mol given in [66]. Also value of a obtained for the fcc lattice is 5.26\AA^{-1} which again is close to the experimental value of 5.31\AA^{-1} [67]

Only the T-NEMD method of analysis is performed for the Argon system. Two models are used to determine the conductivity. Both are constructed from an f.c.c Argon crystal. They are expanded along desired directions so as to obtain the desired geometry. Model I has a system dimension of 78.97 X 18.61 X 18.61 \AA with 960 atoms. It is made periodic along the length so as to mimic the structure of a nanowire. It is similar to the model shown in Fig. 3.4(a). The colored region designates the zone that is heated. Model II is a cube similar to what has been used in [68] except that it is made bigger. It has 864

Table 3.1: System specifications of models used in Zinc Oxide SS-NEMD method

No	System dimensions (Å)	Number of atoms	Surface/Volume (Å^{-1})
I	32.92 X 8.70 X 8.17	320	0.53
II	32.92 X 14.10 X 13.55	720	0.35
III	65.84 X 8.70 X 8.17	640	0.50
IV	98.76 X 8.70 X 8.17	960	0.49

atoms with side of 34.76Å. Fig. 3.4(d) shows the structure of this model. The centrally placed red colored atoms form a spherical region that is chosen as the region of heating. Both systems are energy minimized and pre-equilibrated to 10K and then the temperature is ramped up to 70K (less than melting point of Argon – 83.70K). Finally the system is allowed to cool. T-NEMD analysis is then carried out as described in section II.

3.3.2 Zinc Oxide simulations

Both, SS-NEMD and T-NEMD analysis are performed on the Zinc Oxide system. The layout of this section is as follows. After a brief description of how the structures are generated, the SS-NEMD simulation is described. Here the details of the simulations to compute the conductivity of amorphous and crystalline Zinc Oxide are given. Finally the T-NEMD simulation is described.

A description of the Zinc Oxide force field used in our simulations is described in [58]. Based on the type of method used and the goal, different geometries are generated. The aim of the SS-NEMD method is to determine the variation of thermal conductivity with size; more specifically, the surface/volume (S/V) ratio. S/V ratio has been used as

the parameter to compare thermal conductivity because of its close relation with the thermal scattering of phonons at the surface of nanowires. This effect has been well described in [49]. The aim of the T-NEMD method is to study the effect of periodic boundary conditions. All structures are constructed using the h.c.p unit cell of Zinc Oxide as the starting point. For the SS-NEMD method, the four models are constructed similar to the one shown in Fig. 3.4(a). The regions of heating/ cooling are as shown in Fig. 3.1. A close observation of Fig. 3.4(a) will reveal the equitable distribution of oxygen on top and bottom surfaces of the oxide. This is achieved by shifting half the number of oxygen from the oxygen-rich to the oxygen-poor surface. This ensures that the starting structure is as close as possible; to a real experimental scenario. However unlike an experiment where the sample will have crystal defects, the system under consideration is a perfect crystal. Table 3.2 gives the details of the systems constructed. All systems are one-dimensional periodic along their length.

As described in the theory section, the entire wire is energy minimized and pre-equilibrated to 300K. Then; selected zones are heated / cooled to 500K and 100K respectively. Finally the system is equilibrated at the temperatures mentioned above. No phase change is observed over the range of simulation temperatures. Before a detailed study of the size effect using SS-NEMD is carried out, a general study, to determine if the Zinc Oxide system reproduces the literature values, is performed. The effect of amorphicity of the system on the thermal conductivity is performed on all models

Table 3.2: System specifications of Zinc Oxide models used for T-NEMD method

No	System dimensions (Å)	Number of atoms	Periodicity
I	32.92 X 9.4 X 9.6	320	1D
II	65.84 X 18.78 X 19.22	960	2D
III	63.54 X 27.54 X 22.47	640	3D

To check the influence of crystallinity on thermal conductivity this end we first perform SS-NEMD analysis on systems that are maintained in their perfect crystalline state to determine the conductivity. In another simulation set, the same models are taken through an anneal cycle where they are heated to a high temperature of 2000K (just less than the bulk melting point temperature of Zinc Oxide - 2250K) and then cooled down to 300K using the thermostat. This creates an amorphous system as shown in Fig. 3.4(b). Fig. 3.7 shows the radial distribution function (RDF) plots of the crystalline system as compared to the amorphous system. The radial distribution function - $g(r)$, describes how the density varies as a function of the distance from on particular atom. More precisely, if we consider an atom at the origin and the system is crystalline, then there will be regular occurrence of atoms at periodic intervals and no atoms in between. Hence $g(r)$ will be characterized by peaks and troughs. On the other hand if the system is amorphous where the atoms occur are irregular intervals and hence the peaks will be more spread out. Thus in reference to Fig. 3.7, the presence of a sharp peak on the blue line at about 2Å and then a rapid decay in the number of peaks is an indication of a crystalline structure. The more wider and distributed nature of the red line shows that the system is amorphous. Now, using these systems, the SS-NEMD method was implemented as before.

For the T-NEMD method, three models were constructed to study the effect periodic boundary conditions on the thermal conductivity. Their specifications are mentioned in Table 3.2.

The system is prepared as described in the earlier T-NEMD section. The regions of heating were chosen depending on the boundary condition, heated to 1200K, and allowed to cool. As in the SS-NEMD, no phase change is observed in these simulations as well.

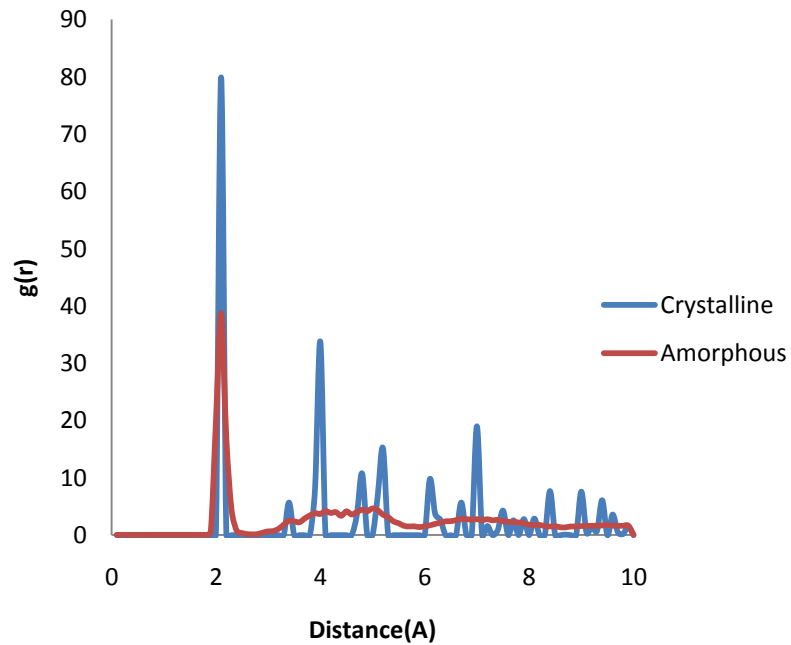


Figure 3.7: Radial distribution function for amorphous and crystalline Zinc Oxide, Zn-O pair

3.4 Results and discussions

3.4.1 Thermal conductivity of Argon

The thermal conductivity derived for model I is shown in Table 3.3. In this case, we see that the obtained values are lower than those in bulk system. The non-periodicity in two-directions gives rise to surface phonon scattering which is known to reduce the conductivity. Also, the expected trend of decreasing thermal conductivity with increasing temperature is reproduced. This trend is an accurate replication of results from Kulkarni and Zhou [49].

This effect is observed due to a decrease in lattice stiffness and reduced phonon mean-free path at higher temperatures. This in turn decreases the heat flux which directly lowers the thermal conductivity of the system. The conductivity for model II and the bulk Argon system is shown in Table 3.4. This system gives higher values than the nanowire system. Moreover, these values are in good agreement with those in literature [68]. The difference between our results and literature may result from the fact that Bhowmick and Shenoy [68] used a Lennard-Jones potential where as ReaxFF uses Morse potential. The error is represented as a standard deviation of the conductivity by taking different regions of the profile.

Table 3.3: Thermal conductivity of Argon wire using T-NEMD method

Temperature (K)	Literature ^[20] (W/m-K)	Conductivity (W/m-K)	Standard deviation
20	1.5	0.65	0.032
30	1.0	0.55	0.015
40	0.60	0.51	0.023
50	0.40	0.50	0.033

Table 3.4: Thermal conductivity of Argon cube using T-NEMD method

Temperature (K)	Literature values ^[19] (W/m-K)	NEMD (W/m-K)	Standard deviation
20	1.50	2.775	0.130
30	1.00	1.538	0.056
40	0.60	0.725	0.001
50	0.40	0.334	0.008

Table 3.5: Thermal conductivity of Zinc Oxide using SS-NEMD method

System description (A)	Thermal conductivity (W/m-K)	Error (%)
32.92 X 9,4 X 9.6 (Crystalline)	1.15	13.2
32.92 X 9,4 X 9.6 (Amorphous)	0.79	39.4
65.84 X 10.2 X 9.4 (Crystalline)	1.33	6.6
65.84 X 10.2 X 9.4 (Amorphous)	0.97	1.3
32.92 X 16.2 X 13.4(Crystalline)	2.21	17.6
32.92 X 16.2 X 13.4(Amorphous)	1.65	5.5
98.76 X 11.4 X11.6 (Crystalline)	1.55	7.8
98.76 X 11.4 X11.6 (Amorphous)	1.07	9.3

3.4.2 Thermal conductivity of Zinc Oxide

Results of the Zinc Oxide SS-NEMD simulation are shown in Table 3.5. The conductivity we are reporting is considered to be at the average temperature of zone between the high and low temperature regions which is 300K in this case.

The conductivities calculated range from 0.79 to 2.2 W/m-K. The expected value based on the Green-Kubo simulations given by Kulkarni [49] is $\sim 3-10$ W/m-K. The lower value is because of the size effect. The S/V ratio used here is between 0.53 and 0.35, whereas Kulkarni *et.al.* [49] uses S/V ratio of 0.21, 0.19 and 0.14. However, we can observe that as the S/V ratio increases, there is a concomitant increase in the conductivity as well. Hence the expected trend is obtained; indicating that, on larger systems will result in higher conductivities. Fig. 3.8 shows the variation of conductivity with S/V ratio at 300K. The trend mentioned above is clearly illustrated in this graph. Also, the thermal conductivity of the crystalline system is consistently higher than that of the amorphous system. This is as expected because the crystalline system being more orderly provides very less impedance to phonon transport in comparison to amorphous system, which are more chaotic.

The errors, calculated based on the deviation of thermal conductivity obtained from the three temperature regions as described in the SS-NEMD method in section II, are around 15% in most cases. The error is large for model I (amorphous) because of small length of the region between the high and low temperature zones. Hence the effects

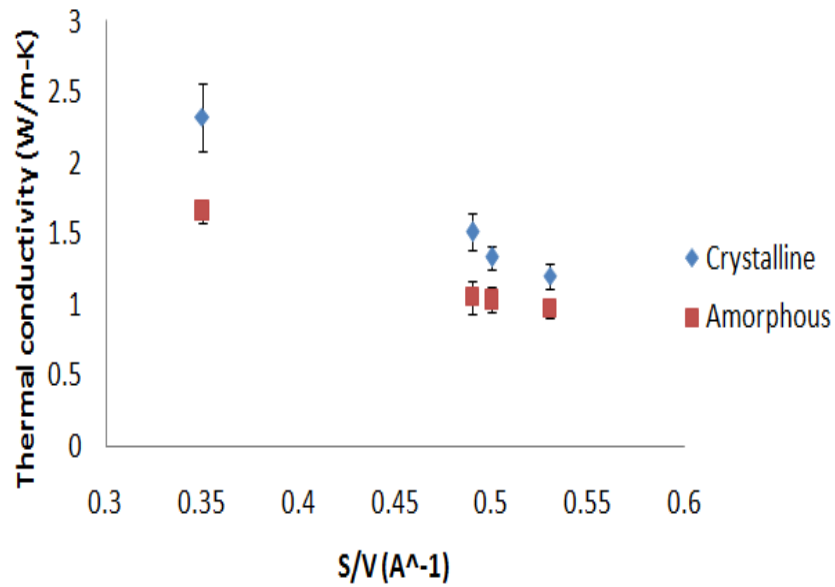


Figure 3.8: Variation of conductivity of Zinc Oxide (Crystalline, Amorphous) with Surface Area to Volume ratio

of the source/ sink are felt throughout the region which prevents a true linear profile from developing. This non-linear profile gives rise to the high error. Increasing the number of atoms or obtaining data from different ensembles will lower the error bars. As mentioned earlier, the asymptotic standard errors associated with the linear interpolation were all found to be less than 10%.

The typical equilibration time required for the SS-NEMD technique is 20ps. This time reduces as the S/V ratio decreased. This is expected as higher conductivity lowers the relaxation time needed. For example, the relaxation time for the amorphous form of model I (S/V=0.53) was about 30ps, where as for model III (S/V=0.35) it was just 17.5ps. Thus the EMD method, in addition to generating the right value of conductivity, also accurately captures the size-effects of the nanowire.

Results of the T-NEMD method for different cases are discussed below. Table 3.5 *gives* the values of the conductivity based on periodicity of the system. As we can see, for the one-dimensional case, the conductivity is of the same order of magnitude as predicted by the SS-NEMD method. The T-NEMD values are closer to those predicted in [49] ($\sim 3-10$ W/m-K). Also the trend of decreasing conductivity with increasing temperature is also obtained in the 1D and 3D cases. A possible reason as to why the 2D case is not following this trend is mentioned below. The experimental value of thermal conductivity for bulk Zinc Oxide from [14] is 116.2 W/m-K, which is in very good agreement with our 3D-result.

The values of conductivity obtained from the NEMD method of a 3D periodic system are close to the experimental value. Thus, we can expect the conductivity of the 2D periodic system to lie in between those of the 1D and 3D cases. This is also obtained correctly. Fig. 3.9 shows all three cases for the purpose of comparison. Here, we are able to clearly distinguish between the 1D, 2D and 3D cases.

The errors for the T-NEMD methods for Zinc Oxide are calculated in the same way as for Argon. Table 3.6 shows the standard deviation for the different cases. If we calculate the percentage error based on the standard deviation, it is about 15% and 10% for the 1D and 3D system respectively. Error for the 2D case is seen to be higher at 20%.

Table 3.6: Thermal conductivity of Zinc Oxide for different periodic boundary conditions using T-NEMD

Temperature (K)	Thermal conductivity (W/m-K)		
	1 D	2 D	3 D
500	6.10±0.9	47.22±7.80	114.26±17.4
600	5.75±0.8	55.88±10.8	115.98±14.6
700	5.29±0.8	62.33±18.8	115.69±12.2
800	4.73±0.7	66.53±20.2	113.75±10.2
900	4.09±0.7	68.43±14.6	110.31±9.92
1000	3.37±0.6	67.96±7.40	105.46±12.6

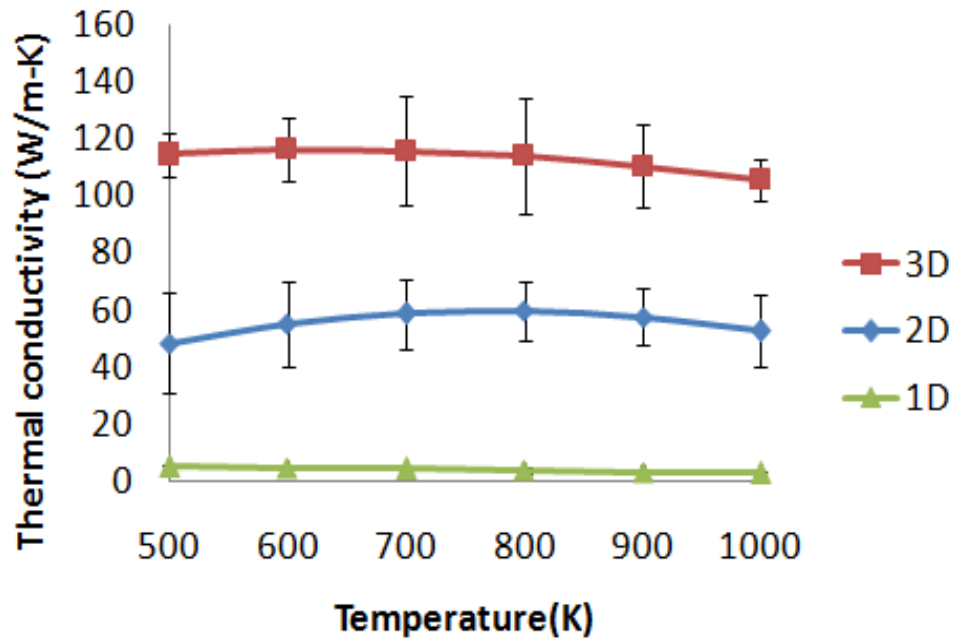


Figure 3.9: Comparison of thermal conductivity of Zinc Oxide method for 1D, 2D and 3D periodic boundary conditions using T-NEMD

The errors in the 2D and 3D systems are likely to be augmented by the interference effects from the neighboring periodic cells in addition to scattering. In a 1D periodic system, this effect is felt only along the length of the wire and since the wire is much longer than the zone of heating, this effect is relatively small. However in the 2D and 3D periodic systems, since the cross-section of the wire is comparable to that of the heating element, these effects may become more significant. For example, in the 2D system, the thickness of the heating element is $5A$ and the cross-section is about $18A$ while for the 1D case, the thickness of the heating element is about $6A$ while the length of the wire is $65.84A$. This may be the reason why the conductivity for the 2D case does not follow the expected trend. Also, in the 2D case, the combination of a lower $S/V = 0.24$ (for 3D system, $S/V = 0.19$), and the surface interference may be the reason for the higher error bars compared to the other cases.

Thus the T-NEMD reproduces the order of the conductivity of Zinc Oxide accurately in all the three cases.

3.5 Sintering

Now that the applicability of the T-NEMD has been established, the method has been extended to predicting the thermal conductivity of sintered Zinc Oxide. Sintering is the process of heating any powder to high temperatures and then cooling it in order to remove any water vapor. The presence of water vapor impedes conductivity. However, by heating the Zinc Oxide particles can coalesce thereby increasing the thermal conductivity. Results for this have been experimentally determined and presented in [48].

Due to limitation of sample size, here we aim to study if ReaxFF can reproduce the experimental trends rather than calculate the thermal conductivity accurately. This is because the small sample size results in large statistical errors in the final result.

3.5.1 Simulation

In order to develop a suitable sample, the experimental approach to sintering was utilized in simulation as well. A Zinc Oxide cluster in a periodic box was equilibrated with water molecules at 300K. The periodic box is compressed by rescaling the velocities of all the atoms for 3ps. The water dissociates on the surface of Zinc Oxides forming hydroxyls Fig. 3.10(a), Fig. 3.10(b). Experimental evidence shows that 50% of surface of Zinc Oxide gets hydroxylated which has confirmed by ReaxFF in earlier simulations by Raymand *et. al* [58][69].

Next, eight such clusters are equilibrated in a periodic box along with water molecules at 300K. This allows the individual clusters to clump together to form a larger

single cluster. The clusters are bound to each other by the hydrogen bonds between the surface hydroxyls as well as some newly formed Zinc Oxygen bonds. The total number of atoms in the system excluding the additionally added water molecules is 1521. Several snapshots from the simulation are shown below in Fig. 3.10 at different stages during material preparation.

Once the sample is prepared, we then proceed to study the effect of sintering. For this purpose, the cluster is equilibrated at a low temperature of 100K. In the first simulation; the cluster in Fig. 3.10(d) is heated to 600K in 12.5ps. In another simulation, the same cluster is heated to a high sintering temperature of 1200K in 25ps. Both clusters are then cooled down back to 100K in 17.5ps and 12.5ps. The final cluster which had been heated to 1200K is henceforth the sintered structure while the former simulation provides the unsintered structure. This is because the high temperature provides enough kinetic energy for the water molecules to escape from the surface of Zinc Oxide thus replicating the process of sintering.

Next, thermal conductivity simulation by the T-NEMD method is carried out. One of the clusters is chosen and is heated to a temperature of 600K using the thermostat by strong coupling (100.0 fs). The other clusters are weakly linked to the thermostat (100000.0 fs). The heating is carried out for 12.5ps for both cases. Once the selected cluster reaches the set temperature, all the clusters are linked to a weak thermostat thereby allowing it to cool naturally. The T-NEMD calculations are then carried out using the thermal transport equation. The spherical form of the equation is used.

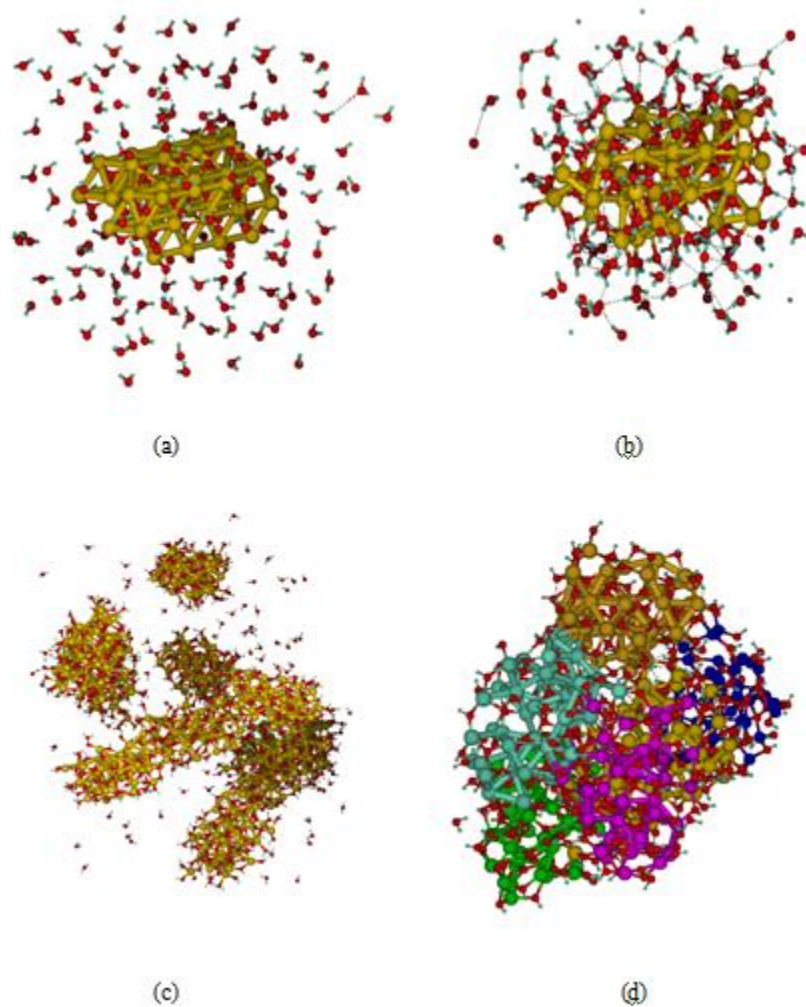


Figure 3.10: Sample preparation for sintering simulation

(a) Equilibration of Zinc Oxide cluster with water, 300K

(b) Equilibrated Zinc Oxide cluster, 300K

(c) Equilibration of six Zinc Oxide clusters with water, 300K

(d) Cluster equilibrated at 300K

A number of test cases are carried out. The cluster is heated to different sintering temperatures, namely – 800K, 1000K, 1200K and 1500K. Another study is done to study the errors associated with the thermal conductivity from the T-NEMD simulation. Five

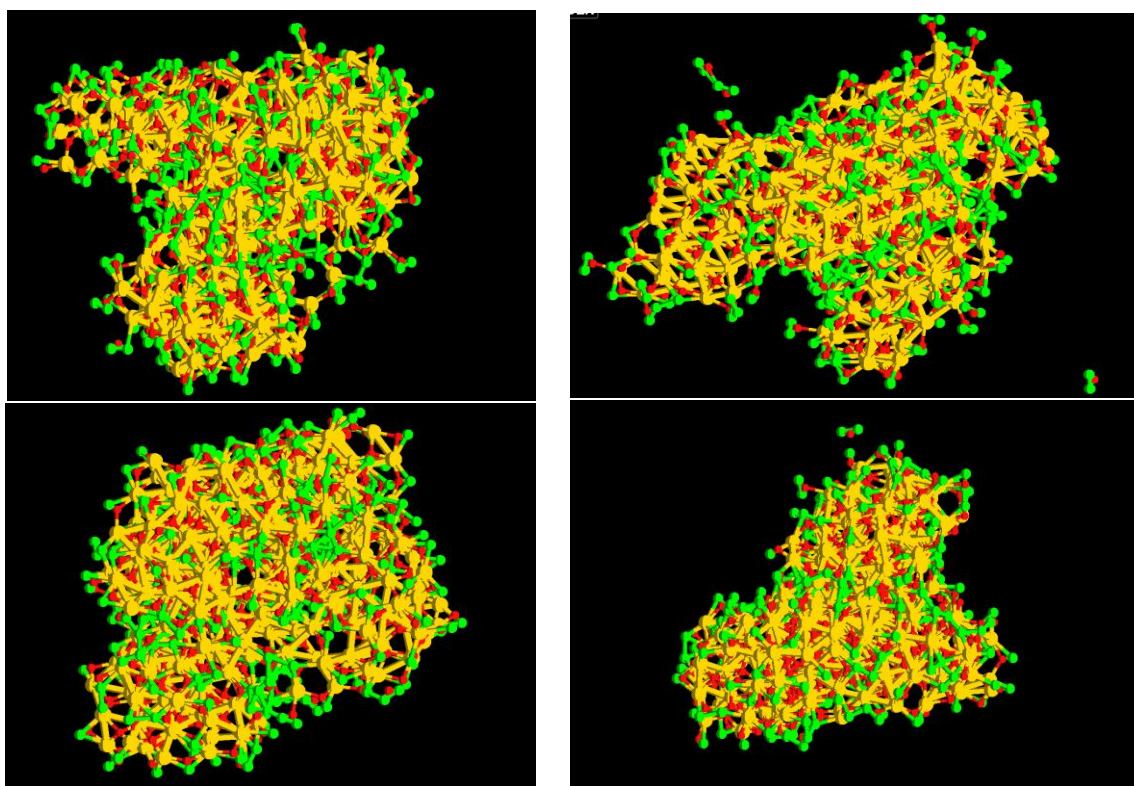


Figure 3.11: Sintered structures at the end of simulation at different anneal temperatures (Top left – 800K, Top right – 1000K, Bottom left – 1200K, Bottom right -1500K)

different simulations are carried out by heating the cluster to 1200K and then cooling it. Standard deviations are calculated for the thermal conductivities obtained this way.

3.5.2 Results and discussion

Refer to Fig. 3.10 (d). The cluster in pink is chosen and strongly coupled to the thermostat. Fig. 3.11 shows the clusters at the end of annealing simulation for different annealing temperatures. The green atoms are the hydrogen, while yellow and red are Zinc

and Oxygen respectively. The intensity of Hydrogen atoms is an indication of the extent of sintering as high temperatures strip the clusters off the hydroxyl bonds. Thus 800K is seen having the maximum intensity of Hydrogen atoms while the 1500K has least of Hydrogen atoms.

Fig. 3.13 shows the temperature variation of blue cluster with time as the pink cluster is heated up. From the graph we see that the higher sintering temperature, the better is the conduction of temperature to the clusters that are weakly coupled to the thermostat. This is because as the temperature increases the number of hydroxyl bonds between the clusters decrease. This implies more connectivity between the clusters in the form of Zinc-Zinc and Zinc-Oxygen bonds.

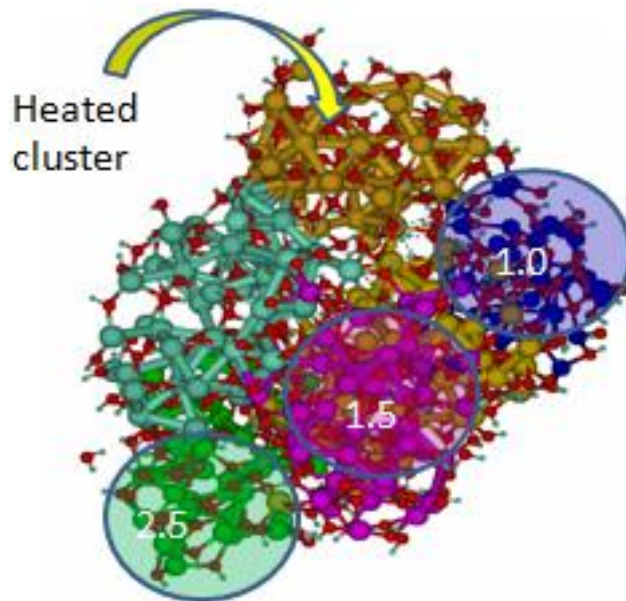


Figure 3.12: Cluster showing the number of grain boundaries, in terms of relative weight, between the heat source and itself

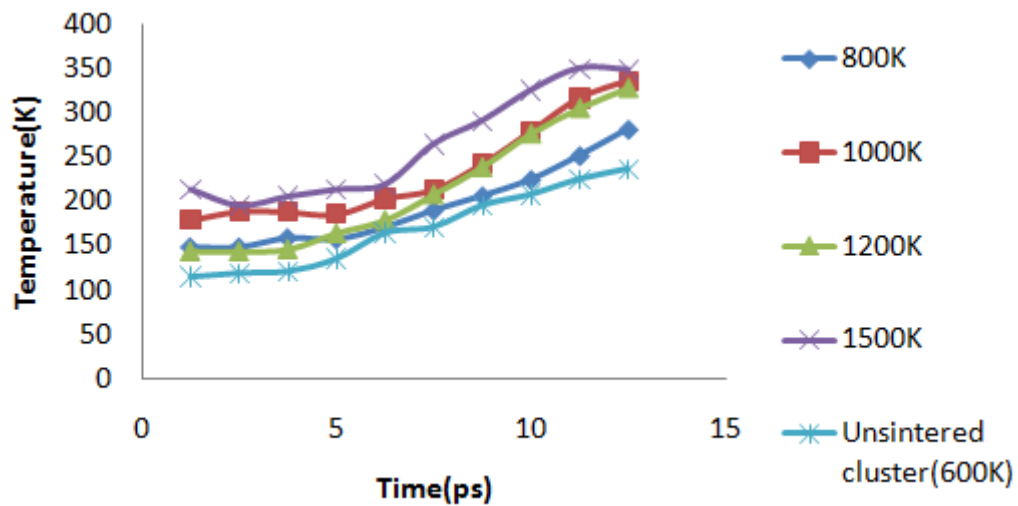


Figure 3.13: Variation of Temperature Vs Time with sintering temperature (Temperature of the green cluster for different sintering temperatures)

Another interesting observation is the temperature difference between the different clusters based on the distance from the heating clusters due to the grain boundaries formed by the hydroxyl bonds between the clusters. Fig. 3.14 shows the variation of temperature with for the different clusters. The number in brackets (in the legend) is a weight. It indicates the number of grain boundaries between the cluster under consideration and the heated/ chosen cluster. As we can see, the temperature is higher in case of the cluster with the list weight.

Fig. 3.15 shows the variation of thermal conductivity with temperature for the sintered and the unsintered case. The sintered structure clearly has a much higher thermal conductivity than compared to the unsintered structure. This is because, as mentioned at the start of this section, the loss of hydroxyl bonds between clusters permits better

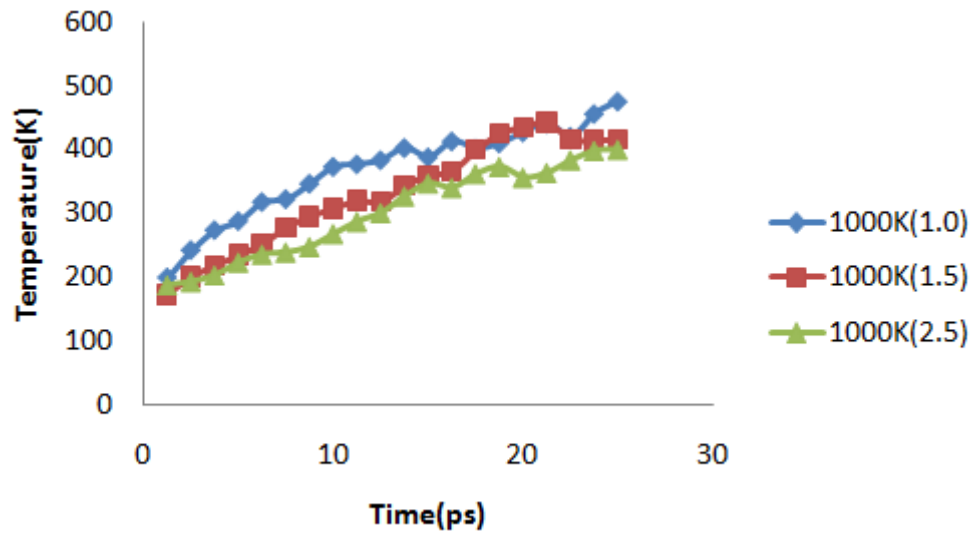


Figure 3.14: Variation of Temperature Vs Time with number of grain boundaries

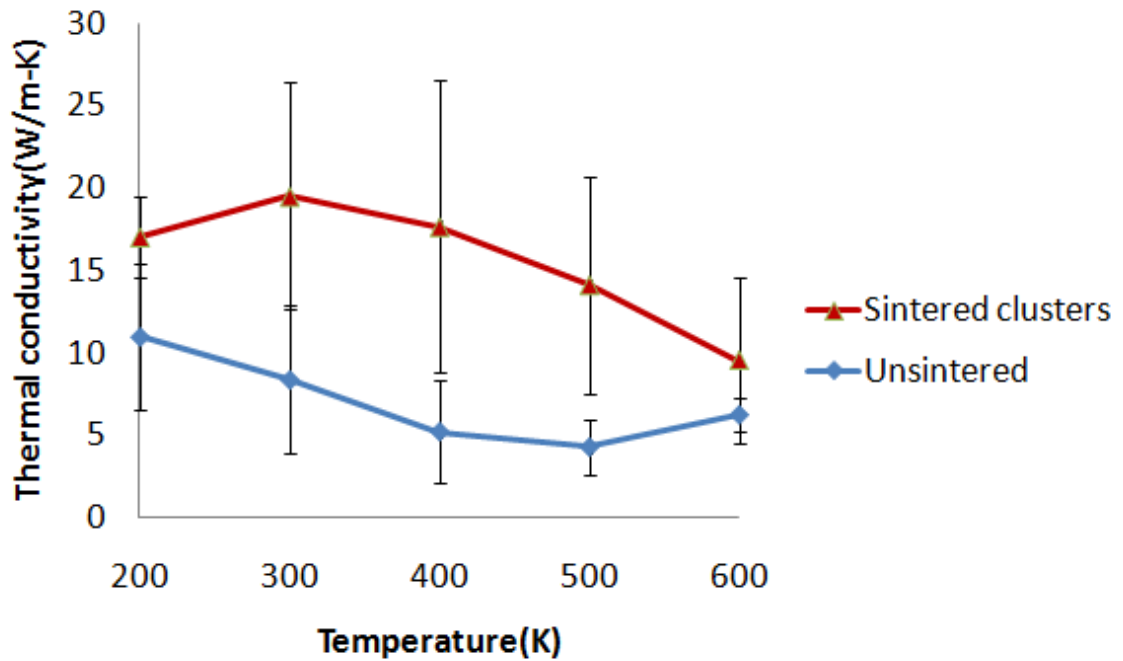


Figure 3.15: Variation of Thermal conductivity Vs Temperature, (sintered and unsintered cases)

conductivity from the source. However, the expected trend of decreasing thermal conductivity with increasing temperature is not observed.

Table 3.7 shows the thermal conductivity value, obtained from the error analysis, when T-NEMD method is applied to the sintered clusters. Table 3.8 shows the same for unsintered clusters. The conductivity values of the sintered cluster, the error on each number is quite high.

Table 3.7: Thermal conductivity of the sintered cluster

Temperature (K)	Thermal conductivity (W/m-K)	% Std. Deviation
200	17.0±6.9	68
300	19.5±8.8	83
400	17.6±6.5	54
500	14.1±5.0	39
600	9.5±6.4	71

Table 3.8: Thermal conductivity of the unsintered cluster

Temperature (K)	Thermal conductivity (W/m-K)	% Std. Deviation
200	9.9±4.4	44
300	11.0±4.5	41
400	8.4±3.11	37
500	5.2±1.6	31
600	6.2±2.9	23

Chapter 4

Conclusions

4.1 Nanowire simulations

We used MD-simulations, using Steady State Non-equilibrium Molecular Dynamics [SS-NEMD] and Transient Non-equilibrium Molecular Dynamics (T-NEMD) methods to determine the 1, 2 and 3-D thermal conductivity of crystalline and amorphous ZnO-systems. In these simulations we used the ReaxFF reactive force field for Zinc Oxide [64]. The SS-NEMD and the T-NEMD methods have their advantages and disadvantages, which are the following.

The SS-NEMD method is confined to a nanowire type structures. More specifically, it is geometry dependent and be applied with good accuracy to arbitrary shapes. It is also affected by system size. However, it has a much shorter simulation time when compared to the Green-Kubo method (total time ~ 30ps) and is much easier to simulate and analyze data using this method. Also it is advantageous when a number of test cases need to be performed.

The T-NEMD method has a distinct advantage over the SS-NEMD method in that it is not confined to any particular geometry. Since most systems can be broken down into 1D case using cylindrical or spherical coordinates, this method can be applied to

sintering clusters and other non-uniform geometries. Also, unlike the SS-NEMD method we are not artificially pumping in/ extracting heat from the system during the cooling simulation. Thus the data from the simulation will not have any skew that is associated with rescaling of velocities. Simulation time is more or less same as that of the SS-NEMD method. However, in order to obtain results within acceptable statistical limits, one must work with relatively larger systems when compared with the SS-NEMD method. The smallest T-NEMD system has 640 atoms whereas the smallest SS-NEMD system has 320 atoms. This in turn increases the run time. In comparison to existing methods, the errors obtained using the T-NEMD method is relatively high. This espouses from the fact that the data from the transient technique has been obtained by averaging over a time ~ 2.5 ps which is a very short averaging time. This is why the errors presented are high and for small systems traditional methods still prevail.

The thermal conductivity of Argon from the T-NEMD method matched those presented in literature [66] thereby verifying the validity of this method. The higher conductivity of the bulk system as compared to the nanowire indicates that the periodicity of the system results in significant loss of thermal conductivity.

The thermal conductivity of Zinc Oxide using the SS-NEMD methods for the different cases is found at 300K. The conductivity of the amorphous systems is found to be lower than those of the pure crystalline systems. Also, the conductivity is found to vary significantly with size of the system, more specifically with the surface-to-volume

ratio of the system. As the S/V ratio decreased, i.e. as the system tended more towards bulk, the thermal conductivity increased.

The effect of system periodicity is studied using the T-NEMD method. The conductivity increased by a factor of ten from one to two to three dimensional periodicity. The 1D system had a conductivity of ~3-6 W/m-K. The 2-D system had a conductivity of ~50-70 W/m-K and the 3D system had a conductivity of approximately 105-116 W/m-K. This fact was also verified physically by comparing their cooling times. The 3D system was found to cool under 3ps while the 2D system required around 4ps. The 1D system required a much longer time of ~15ps. Also, the effect of temperature on conductivity was also reproduced by this method. As the temperature increased the thermal conductivity decreased.

Overall, this work demonstrates that the SS-NEMD and T-NEMD methods, in conjunction with the ReaxFF description, allow us to accurately calculate thermal conductivity values for 1, 2 and 3-dimensional systems. This, combined with the ability of the ReaxFF method for simulating surface chemistry, makes this method into a very attractive tool for establishing the thermal conductivity effects associated with sintering, sensor and catalysis.

4.2 Sintering simulations

The results from the sintering simulation show that ReaxFF can be used to simulate chemical reactions like sintering. The aggregation of the clusters with the hydroxyl bonds and their eventual loss in the form of water by raising the temperature of the system replicates experimental observation.

Thermal conductivity study performed also concurs with the literature trends from [14]. The literature values themselves however have relatively large error bars. This is because of the small system size. Just as we observed in the SS-NEMD simulation results for Zinc Oxide, a better value of conductivity with lower error bars can be obtained using lower surface area to volume ratio.

The thermal conductivity of the sintered Zinc Oxide is higher than that of the unsintered cluster due to the absence of the hydroxyl bonds between the Zinc Oxide clusters. Cluster temperature (a group of atoms far away from the heat source) increases as the sintering temperature increases reaffirming the above observations. Also, the temperature of the clusters decreased as the distance from the heat source increased due to the grain boundary scattering. This shows that the hydroxyl bonds act as thermal impedance to the thermal conductivity.

Thus in conclusion, ReaxFF reactive force field can be used to study the chemical reactions and its effect on mechanical properties like including thermal conductivity.

4.3 Future work

Thermal transport research offers a lot of scope for simulation and experimental research. ReaxFF, in particular, with its ability to simulate chemistry of reactions, further expands the gamut of applications where the steady state and transient thermal conductivity can be used.

Large scale sintering simulation, with system size exceeding 10,000 atoms, can be performed. This will give a better insight in to the effect that sintering has on thermal conductivity. Also, the current code to calculate the conductivity is only first order accurate in time. This can be extended to higher orders of accuracy to yeild better results.

Another interesting extension is the study failure of nanowires. Under tensile stress, nanowires break along preffered planes. Strain is found to have an impact on the thermal conductivity of the system as described in [50]. Studying the effect that different chemical environments have on the failure of the nanowire is a more practical study as nanowires are seldom placed in vaccuum. Presence of oxidising agents like water and ammonia are expected to alter the failure stress significantly. They may also indirectly affect the thermal conductivity. This provides novel avenues for application of nanowire in sensor technology.

A topic that is receiving a lot of attention these days is the study of grain boundaries on electrical and thermal conductivity. This is because, even though perfectly crystalline Zinc Oxide can be manufactured [12], nanowires tend to accrue defects over

their lifetime. Formation of internal defects such as vacancies, local amorphization and grain boundary formation adversely affect the performance and utility of the nanowires. Unfortunately, studying these defects experimentally is extremely difficult as these defects lie inside the bulk of the wire and hence can be analyzed only through invasive procedures. ReaxFF, and other simulation methods in general, offer a way to circumvent this problem. Studying thermal conductivity and Kapitza resistance properties [57] of different grain boundaries would make an interesting study.

The above mentioned scenarios are only a few of the wide range of possibilities. On the whole, ReaxFF combined with the thermal conductivity methods presented in this thesis opens the doors to numerous other avenues of research and application.

BIBLIOGRAPHY

1. Mongillo J. F., 'Nanotechnology 101', Chap. 10, Greenwood Press, London (2007)
2. Hornyak G. L., Tibbals H. F., Dutta J., Moore J. J., 'Introduction to nanoscience and nanotechnology', Chap. 1-3, CRC Press, FL USA (2009)
3. Thomson W., 'Kinetic Theory of the Dissipation of Energy', *Nature*, 9, pp. 441-444 (1874)
4. Thomson W., 'The Sorting Demon of Maxwell', *Proceedings of the Royal Institution of Great Britain*, vol. ix, pp. 113 (1879)
5. Weber A. S. 'Nineteenth Century Science: A Selection of Original Texts', pp.300, Broadview Press, Orchard Park NY (2000)
6. Leff H. S., Rex A. X., 'Maxwell's Demon: Entropy, Information and Computing', pp.4, Princeton University Press, Great Briton (1990)
7. Zsigmondy R., 'Colloids and the Ultramicroscope', J.Wiley and Sons, NY, (1914)
8. Feynman R. P., 'The Feynman Lectures on Physics, Vol. 1. Massachusetts', Chap. 46, Addison-Wesley, USA (1963)
9. Taniguchi N., 'On the Basic Concept of 'Nano-Technology'', *Proc. Intl. Conf. Prod. Eng. Tokyo- Part II*, Japan Society of Precision Engineering (1974)
10. Marshall J., 'What is nanotechnology?' <http://nanotechnology.cm/posts> (2010)
11. Schmid G., Maihack V., Lantermann F., Peschel S., *J. Chem. Soc. Dalton Trans.*, vol. 589 (1996)
12. Wang Z. L., 'Zinc Oxide nanostructures: growth, properties and application', *Journal of Physics: Condensed Matter*, 16, R829-R858 (2004)
13. Klabunde K. J., 'Nanoscale Materials in Chemistry', Wiley InterScience, New York NY (2001)
14. Özgür, Ü., Alivov Ya. I., Liu, C., Teke, A., Reshchikov, M. A., Doğan, S., Avrutin, V., Cho, S. J. 'A comprehensive review of ZnO materials and devices', *Journal of Applied Physics*, vol. 98 (2005)

15. Parrinello M., Rahman A., 'Crystal structure and pair potentials: A molecular dynamics study' *Phys. Rev. Lett.*, vol. 45, pp. 1196-1199 (1980)
16. Parrinello M., Rahman A., 'Polymorphic transitions in single crystals: A new molecular dynamics method', *J.Appl.Phys.*, vol. 52, pp.7182-7190 (1981)
17. Berendsen H. J. C., Postma J. P. M., van Gunsteren W. F., Dinola A., Haak J. R., 'Molecular-Dynamics with Coupling to an External Bath', *Journal of Chemical Physics*, vol. 81, pp.3684-3690 (1984)
18. Brenner D. W., 'Empirical potential for hydrocarbons for use in simulating the chemical vapor deposition of diamond films'. *Phys. Rev. B* 42 (15): 9458 (1990)
19. van Duin A. C. T., Dasgupta S., Lorant F., Goddard III W. A., 'ReaxFF: A Reactive Force Field for Hydrocarbons', *J. Phys. Chem. A* **105**: 9398 (2001)
20. Swope W. C., Andersen H. C., Berens P. H., Wilson K. R., 'A computer simulation method for the calculation of equilibrium constants for the formation of physical clusters of molecules: application to small water clusters', *J. Chem. Phys.*, vol. 76, pp. 637-649 (1982)
21. Berendse H. J. C., Postma J. P. M., van Gunsteren W. F., Dinola A., Haak J. R., 'Molecular-Dynamics with Coupling to an External Bath'. *Journal of Chemical Physics*, vol. 81, pp. 3684-3690 (1984)
22. Andersen H. C., 'Molecular Dynamics at constant pressure and/or temperature', *J.Chem. Phys.*, vol. 72, pp.2384-2393 (1980)
23. Hoover W. G., 'Canonical dynamics: Equilibrium phase-space distributions', *Phys.Rev. A*, vol. 31, pp.1695-1697 (1985)
24. Hoover W. G., 'Constant pressure equations of motion', *Phys. Rev. A*, vol. 34, pp.2499-2500 (1986)
25. Zhu, R., Janetzko, F., Zhang, Y., van Duin, A. C. T., Goddard W. A., Salahub D. R., 'Characterization of the active site of yeast RNA polymerase II by DFT and ReaxFF calculations', *Theoretical Chemical Accounts*, vol. 120, pp.479-489 (2008)
26. van Langeveld A. D., van Duin A. C. T., Bijsterbosch J. W., Kapteijn F., Moulijn J. A., 'Correlation of bulk and surface thermodynamics of some transition-metal oxides - applications to exhaust-gas catalysts', *Stud. Surf. Sci. and Catal.*, vol. 75, pp.2693-2696 (1993)
27. Lai W., Song C., van Duin A. C. T., de Leeuw J. W., 'Ring-shift isomerization of [sym]-octahydrophenanthrene into [sym]-octahydrophenanthrene. Effects of

- zeolite catalysis and equilibrium compositions' *Catal. Today*, vol. 31 (1-2), pp.145-161 (1996)
28. van Duin A. C. T., Baas J. M. A., van de Graaf B., de Leeuw J. W., Bastow T. M., Alexander R., 'Comparison of calculated equilibrium mixtures of alkylnaphthalenes and alkylphenanthrenes with experimental and sedimentary data; The importance of entropy calculations' *Org. Geochem.*, vol 26, pp. 275-280 (1997)
 29. Nielson K. D., van Duin A. C. T., Oxgaard, J., Deng W., Goddard III W. A., 'Development of the ReaxFF reactive force field for describing transition metal catalyzed reactions, with application to the initial stages of the catalytic formation of carbon nanotubes.', *J. Phys. Chem. A.*, vol. 109, pp.493-499 (2005)
 30. Buehler M. J., Tang H., van Duin A. C. T., Goddard W. A., 'Threshold crack speed controls dynamical fracture of silicon single crystals', *Physical Review Letters*, vol. 90, pp. 65502 (2007)
 31. Ludwig, J., Vlachos, D. G., van Duin A. C. T. and Goddard, W. A., 'Dynamics of the dissociation of hydrogen on stepped platinum surfaces using the ReaxFF reactive force field' *Journal of Physical Chemistry B*, vol. 110, pp.4274-4282 (2006)
 32. Alder B. J., Wainwright T. E. 'Phase Transition for a Hard Sphere System". *J. Chem. Phys.*, vol. 27: 1208-1209 (1957)
 33. Alder B. J., Wainwright T. E, 'Phase Transition in Elastic Disks'. *Phys. Rev.*, vol. 127, pp.359-361 (1962)
 34. Rahman A., 'Correlations in the motion of Argon', *Phys. Rev.*, 136:2, A405 – A411 (1964)
 35. Stillinger F. H., Rahman A., 'Propagation of sound in water: a molecular dynamics study', *Phys. Rev. A*, Vol. 10, Issue 1, pp.368-378 (1974)
 36. McCammon J. A., Gelin B. R., Karplus M., 'Dynamics of folded proteins', *Nature*, 267, pp.585-590 (1977)
 37. Yung P., Yun H., Mao S., Russo R., Johnson J., Saykally R., Morris N., Pham J., He R., Choi R., 'Controlled growth of Zinc Oxide and their optical properties', *Adv. Funct. Mater.*, vol.12, pp.323-331(2002)
 38. Goldberger J., Kim F., Johnson J. C., Zhang Y., Saykally R. J., Yang P., 'Low-Temperature Wafer-Scale Production of ZnO Nanowire Arrays', *Angew. Chem. Int. Ed* 42, (26): 3031-3032 (2003)

39. Pacholski C., Kornowski A., Weller H., 'Self-assemble of ZnO: From nanodots to nanorods', *Angew. Chem. Int. Ed.*, vol.41 (7), pp.1188 – 1191(2002)
40. Venkatachalam S., Kanno Y., 'Preparation and characterization of nano and microcrystalline ZnO thin films by PLD', *Current Applied Physics*, vol. 9 (6), pp.1232-1236 (2009)
41. Shao J., Shen Y. Q., Sun J., Xu N., Yu D., Lu Y. F., Wua J. D., 'Low-temperature *c*-axis oriented growth of nanocrystalline ZnO thin films on Si substrates by plasma assisted pulsed laser deposition', *Journal of Vacuum Science and Technology B (Microelectronics and Nanostructures)*, v 26, n 1, pp.214-218 (2008)
42. Zhang Y., Lin B., Fu Z., Liu C., Han W., 'Strong ultraviolet emission and rectifying behavior of nanocrystalline ZnO films', *Opt. Mater.*, v 28, n 10, pp.1192-1196 (2006)
43. Zhang X.T., Liu Y.C., Zhi Z.Z., Zhang J.Y., Lu Y.M., Xu W., Shen D.Z., Zhong G.Z., Fan X.W., Kong X.G., 'High intense UV-luminescence of nanocrystalline ZnO thin films prepared by thermal oxidation of ZnS thin films', *J. Cryst. Growth*, v. 240, n 3-4, p463-436 (2002)
44. Min G., Peng D., Shengmin C., 'Hydrothermal growth of perpendicularly oriented ZnO nanorod array film and its photoelectrochemical properties', *Appl. Surf. Sci.*, v. 249, n 1-4, pp.71-75 (2005)
45. Zhang Z. M., 'Nano/Microscale heat transfer', Chap 6, McGraw-Hill, New York, (2007)
46. Ozgur U., Gu X., Spradlin J., Cho S. J., Morkoc H., Pollock F. H., Nemeth B., Nause J., 'Thermal conductivity of bulk ZnO after different thermal treatments', *Journal of the Electrochemical Materials*, v35, n 4, pp.550-555 (2006)
47. Florescu D. I., Mourikh L. G., Pollak Fred H., Look D. C., Cantwell G., Li X., 'High spatial resolution thermal conductivity of bulk Zinc Oxide', *Journal of Applied Physics*, 91 (2), pp.890-892 (2006)
48. Olorunyolemi, T., Birnboim A., Carmael Y., Wilson O.C., Jr. Loyd, I.K., 'Thermal conductivity of Zinc Oxide from green to sintered state', *Journal of American Ceramic Society*, v 85, n 5, pp.1249-1253 (2002)
49. Kulkarni A. J. Zhou M., 'Size-dependent thermal conductivity of Zinc-oxide nanobelts', *Applied Physics Letters*, v 88, n 14, pp.141921-1-3 (2006)
50. Kulkarni A. J, Zhou M., 'Tunable thermal response of ZnO nanowires', *Nanotechnology*, 18 (2007) 435706 (6pp)

51. W. G. Hoover, 'Computational Statistical Mechanics', Elsevier, Amsterdam, (1991)
52. Schelling P. K., Phillpot S. R., Keblinski P., 'Comparison of atomic –level simulation methods for computing thermal conductivity', *Physical Review B*, v 65, n 14 144306/1-12 (2002)
53. Righini F., Bussolino G. C., Rosso A., Roberts R. B., 'Thermal conductivity by a Pulse-Heating Method: Theory and experimental apparatus', *International Journal of Thermophysics*, 11 (4), pp.629-641 (1990)
54. Feng B., Li Z., Zhang X., 'Effect of grain boundary scattering on thermal conductivity of nanocrystalline metallic films', *J. Phys. D: Appl. Phys.*, v 42, n 5, p055311 (5pp.) (2009)
55. Yan K., Soh Ai-Kah, 'Effect of grain boundary cavities on the thermal resistance under ultrashort laser pulse', *J. Phys. D: Appl. Phys.* 41,155401 (8pp) (2008)
56. Schelling P. K., Phillpot S. R., Keblinski P., 'Kapitza conductance and phonon scattering at grain boundaries by simulation', *J. Appl. Phys.* 95 6082 (2004)
57. Maiti A., Mahan G. D., Pantelides S. T., 'Dynamical simulations of nonequilibrium processes—heat flow and Kapitza resistance across grain boundaries', *Solid State Commun*, 120 517 (1997)
58. Raymand D., van Duin A. C. T., Baudin M., Hermansson K., 'A reactive force field for Zinc Oxide', *Surface Science*, **602** (5) , pp.1020–1031 (2008)
59. Catti M., Noel Y., Dovesi R., 'Full piezoelectric tensors of wurtzite and zinc blende ZnO and ZnS by first-principles calculations', *J. Phys. Chem. Solids*, v 64, n 11, pp.2183-2190 (2003)
60. Serrano J., Romero A., Lauck F., Cardona M., Rubio A., 'Pressure dependence of the lattice dynamics of ZnO: an ab-initio approach', *Phys. Rev. B (Condensed matter)*, v 69, n 9, 94306-1-14 (2004)
61. Yu Z.G., Gong H., Wu P., 'Theoretical and experimental studies on oxygen vacancy in p-type ZnO', *J. Cryst. Growth*, v401-402, pp.417-420 (2007)
62. Lee C., Yang W., Parr R., 'Development of the Colle-Salvetti correlation-energy formula into a functional of the electron density', *Phys. Rev. B*, vol. 37, n 2, pp.785-789 (1988)
63. Becke A. D., 'Density-functional thermochemistry. III. The role of exact exchange', *J. Chem. Phys.*, vol. 98, pp.5648-5652 (1993)

64. Dick B., Overhauser A., 'Theory of the Dielectric Constants of Alkali Halide Crystals', *Phys. Rev.*, vol. 112, Issue 1, pp.90-103 (1958)
65. Yao B. D., Chan Y. F., Wang N., 'Formation of ZnO Nanostructures by simple way of thermal evaporation', *Appl. Phys. Lett.*, v 81, n 4, pp.757-759 (2002)
66. Greenwood N. N., Earnshaw A., 'Chemistry of the Elements (2nd ed.)', pp.891 Butterworth-Heinemann, Oxford (1997)
67. Lukes J. R., Li D. Y., Liang X. G., Tien C. L., 'Molecular Dynamics Study of solid thin-film thermal conductivity', *Journal of Heat Transfer*, 122 (3), pp.536-548 (2000)
68. Bhowmick S., Shenoy V. B., 'Effect of strain on the thermal conductivity of solids', *Journal of Physics*, v 125, n 16, p16545-1-3 (2006)
69. Raymand D., van Duin A. C. T., Baudin M., Hermansson K., 'Water adsorption on stepped ZnO surfaces from MD simulation', *Surface Science*, vol. 604, Issue 9-10, pp.741-752 (2010)

APPENDIX-A

Temperature Calculation (fortran77)

```
PROGRAM Temp_profile
!This code reads in atom coordinates at every time step and calculates the temperature
!based on Kinetic energy. It then averages the temperatures over a specified number of
!iterations.
    IMPLICIT NONE
! Variable declaration
    REAL          :: xold(No),yold(No),zold(No)
    REAL          :: xnew(No),ynew(No),znew(No)
    REAL          :: Mh,Mzn,Mo,dt,R
    INTEGER       :: n,No
    CHARACTER*2   :: atoms(No),dummy
    INTEGER       :: i,j,k,l,sf,skip,counternew,counterold
    REAL         :: xvel(No),yvel(No),zvel(No)
    REAL         :: vel(No),KE(No)
    REAL         :: T(No,20000),Tsum(No)
    REAL         :: dummy,Tavg(No)
    PARAMETER(n=20000,No=7786,Mzn=63.50e-03,Mo=16.00e-03)
    PARAMETER(Mh=1.00794e-03,R=8.31450,dt=0.25)

! where      Mzn      - mass of Zinc (g)
!            Mo       - mass of Oxygen (g)
!            Mh       - mass of Hydrogen (g)
!            R        - Universal gas constant
!            dt       - time step
!            (x,y,z)old - atom coordinates at current time step
!            (x,y,z)new - atom coordinates at new time step
!            n        - number of iterations
!            No       - number of atoms in the system
!            atoms    - atom type
!            dummy    - dummy variable
!            i,j,k,l,sf - counters
!            counternew,counterold - counters
!            (x,y,z)vel - velocity components in the x,y,z direction
!            vel      - net velocity
!            T        - Temperature
!            KE       - Kinetic energy
```

```

!           Tsum          - Sum of temperatures of individual atoms over all frames
!           Tavg          - Average temperature of the atom
!           xmolout       - contain atom coordinates at each time step (.xyz format)

```

```

OPEN(UNIT = 2,FILE = 'xmolout')
READ(2,99)
DO i = 1,No
    READ(2,101)dummy
ENDDO

```

```

! To skip the first n-frames
sf = 000000
skip = sf*(No+2)/2
OPEN(UNIT = 1, FILE ='xmolout')
DO i=1,skip
    READ(1,99)
READ(2,99)
ENDDO

```

```

!Reading atom coordinates

```

```

DO l = 1,n-1

```

```

!Reading in frames

```

```

    READ(1,99)
    READ(2,99)
    counternew = counternew + 1
    DO j = 1,No
        READ(1,100) atoms(j),xold(j),yold(j),zold(j)
        READ(2,100) atoms(j),xnew(j),ynew(j),znew(j)

```

```

        CONTINUE

```

```

    ENDDO

```

```

!Calculating velocity

```

```

    DO j=1,No
        ! x component
        xvel(j)= (xnew(j)-xold(j))*10**5/(dt)
        ! y component
        yvel(j)= (ynew(j)-yold(j))*10**5/(dt)
        ! z component
        zvel(j)= (znew(j)-zold(j))*10**5/(dt)
        ! net velocity
        vel(j) = (xvel(j)**2+yvel(j)**2+zvel(j)**2)**0.5
    ENDDO

```

```

!Calculating temperature
      DO j = 1,No
          IF(atoms(j)=='Zn')THEN
              KE(j)=0.5*Mzn*vel(j)**2
          ELSEIF(atoms(j)=='O')THEN
              KE(j)=0.5*Mo*vel(j)**2
          ELSEIF(atoms(j)=='H')THEN
              KE(j)=0.5*Mh*vel(j)**2
          ENDIF
          T(j,1) = 2.0/3.0*KE(j)/R
      ENDDO
ENDDO

      DO i = 1,No
          Tsum(j) = 0.0
      ENDDO
!Calculating block sum temperature
      DO i = 1,No
          DO j = 1,(n-1)
              Tsum(i) = Tsum(i) + T(i,j)
          ENDDO
          Tavg(i) = Tsum(i)/(j-1)
      ENDDO

!Outputing average
      OPEN(UNIT = 3, FILE='blockavg.txt')
      DO i = 1,No
          WRITE(3,102)i,Tavg(i)
      ENDDO

      99 FORMAT(/)
      100 FORMAT(A2,3(1X,F9.5))
      101 FORMAT(3X,F9.5)
      102 FORMAT(I4,5X,F16.8)

      END PROGRAM

```

APPENDIX B

Calculation of thermal conductivity – Cartesian coordinates (MATLAB)

```
% This program loads the averaged temperatures over time and space (contained in
% blockavg.txt), curve fits this data to second order polynomial and calculates the thermal
% conductivity by solving the Cartesian form of the Heat conduction equation using the
% overdetermined least squares method.
% Loading file
clear all;
t=load('blockavg.txt');
% Format of blockavg.txt:
% 1st column – atom coordinates along length of the nanowire
% 2nd column onwards – Corresponding averaged atom temperatures
% -----
% selecting region
n=640;           % number of atoms
ll=50;          % starting point for temperature profile
ul=300;         % ending point for temperature profile
T=500;         % Temperature
selx=ll*0.1:0.1:ul*0.1; % atom coordinates
% -----
% forcing symmetry into the profile
for i=2:6
    for j=1:n/2
        t1(j,i)=(t(j,i)+t(n-j+1,i))/2;
        t1(n-j+1,i)=t1(j,i);
    end
end
t1(:,1)=t(:,1);
tt1=t1';
% -----
% assigning temperatures in the selected region
for i=2:6
    for j=1:ul-ll+1
        k1=i-1;
        k2=j;
        selt(k1,k2)=tt1(i,j);
    end
end
% -----
% fitting for time and space
% fitting curve for space
```

```

for i=1:5
    [p,s]=polyfit(selx,selt(i,:),2);
    q(i,1)=p(1);
    q(i,2)=p(2);
    q(i,3)=p(3);
end
%fitting curve for time
delt=(1.5:3:13.5);
for i=1:ul-ll+1
    for j=1:5
        [r,u]=polyfit(delt',selt(:,i),2);
        v(1,i)=r(1);
        v(2,i)=r(2);
        v(3,i)=r(3);
    end
end
%-----
%plotting graph
delt1=delt;
time1(1:4,1:300)=0;
time1(1,:)=delt(1);
time1(2,:)=delt(2);
time1(3,:)=delt(3);
time1(4,:)=delt(4);
time1(5,:)=delt(5);
selr1=selx;
f11=polyval(q(1,:),selr1);
f21=polyval(q(2,:),selr1);
f31=polyval(q(3,:),selr1);
f41=polyval(q(4,:),selr1);
f51=polyval(q(5,:),selr1);
plot3(time1(1,:),selr1,f11,time1(2,:),selr1,f21,time1(3,:),selr1,f31,time1(4,:),selr1,f41,time1(5,:),selr1,f51)
%-----
%evaluation derivatives
%evaluating first derivative
for i=1:5
    for j=1:ul-ll+1
        fd(i,j)=2*q(i,1)*selx(j)+q(i,2);
    end
end
%evaluating second derivative
for i=1:5
    for j=1:ul-ll+1
        sd(i,j)=2*q(i,1);
    end
end

```



```

        end
    end
    %evaluating time derivative
    for i=1:5
        for j=1:ul-ll+1
            k=(ul-ll+1)*(i-1)+j;
            ftd(k,1)=2*delt(i)*v(1,j)+v(2,j);
        end
    end
    %-----
    %Setting up coefficients
    for i=1:5
        for j=1:ul-ll+1
            k1=(ul-ll+1)*(i-1)+j;
            coa1(:,k1)=sd(i,j);
            coa2(:,k1)=selt(i,j)*sd(i,j)+fd(i,j)^2;
            coa3(:,k1)=selt(i,j)^2*sd(i,j)+2*selt(i,j)*fd(i,j)^2;
        end
    end
    %-----
    %Setting up coefficient matrix and rhs matrix
    comat(:,1)=coa1';
    comat(:,2)=coa2';
    comat(:,3)=coa3';
    ro=5675*10^-30;
    Cp=(53.999+0.0007851*T-5.868*10^5/T^2-127.5/sqrt(T)+1.9376*10^-
    6*T^2)*81.39;%(multiply by molecular mass)
    %-----
    %overdetermined method of least squares
    comat1=comat'*comat;
    ftd1=comat'*ftd;
    rhs=ro*Cp*ftd1;
    %-----
    %calculating unknowns
    coeff=comat1\rhs;
    kapp=coeff(1)+coeff(2)*T+coeff(3)*T^2;
    kappa=kapp*10^22
    %-----

```

APPENDIX C

Data preparation for Cylindrical and Spherical Heat Conduction equation (MATLAB)

% This code is used to prepare data for solving the heat conduction equation in cylindrical
% and spherical form. It reads in the file 'blockavg.txt' and averages the temperatures of
% all the atoms that are at equal distance from a chosen central atom. This gives the
% temperature distribution of the wire as a function of radial distance

% Loading file

```
t=load('blockavg.txt');
```

% Format of blockavg.txt:

% 1st column – Distance of atom from the chosen central atom (radius)

% 2nd column onwards – Corresponding averaged atom temperatures

% -----

% Some definitions

```
maxr=max(t(:,2)); % Maximum radius
```

```
minr=min(t(:,2)); % Minimum radius
```

```
r=t(:,2); % Radius
```

```
No=2560; % Total number of atoms
```

```
cent=2488; % Central atom
```

```
profs=3; % Starting time profile
```

```
profe=7; % Ending time profile
```

```
nop=profe-profs+1; % Number of profile
```

```
binsize=1.0; % Size of bin
```

```
binno=round((maxr-minr)/binsize); % Bin number
```

% -----

% Sorting atoms into bins on radii

```
binc(1:binno) = 0;
```

```
ll=0;
```

```
ul=binsize;
```

```
for j=1:binno
```

```
    for k=1:No
```

```
        if((r(k)<ul)&&(r(k)>=ll))
```

```
            binc(j) = binc(j) + 1;
```

```
        end
```

```
    end
```

```
    ll=ll+binsize;
```

```
    ul=ul+binsize;
```

```
end
```

% -----

% Calculating total bin temperature

```
l=1;
```

```
f=0;
```

```
ll=0.0;
```

```

ul=binsize;
tsum(1:binno,1:nop) = 0;
for i=profs:profe
    for j=1:binno
        for k=1:No
            if((r(k)<ul)&&(r(k)>=ll))
                tsum(j,1)= t(k,i)+tsum(j,1);
                f=f+1;
            end
        end
        ll=ll+binsize;
        ul=ul+binsize;
    end
    l=l+1;
    ll=0;
    ul=binsize;
end
%-----
% Calculating the average
tavg(1:binno,1:nop)=0;
for i=1:nop
    for j=1:binno
        tavg(j,i)=tsum(j,i)/binc(j);
    end
    l=l+1;
end
%-----
% To plot graphs
ser=binsize:binsize:maxr;
selr=ser';
plot(ser,tavg(:,1),ser,tavg(:,2),ser,tavg(:,3),ser,tavg(:,4),ser,tavg(:,5))
%-----
% Writing output
%save tavg.txt tavg -ASCII

```